

**DURABILITY ASSESSMENT AND MODELING OF WOOD-THERMOPLASTIC
COMPOSITES**

By

SUDARSHAN RANGARAJ

A thesis submitted in partial fulfillment of
the requirements for the degree of

MASTER OF SCIENCE IN MECHANICAL ENGINEERING

WASHINGTON STATE UNIVERSITY
School of Mechanical and Materials Engineering

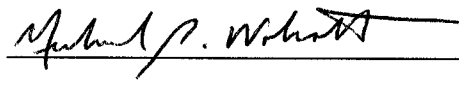
August 1999

To the Faculty of Washington State University:

The members of the Committee appointed to examine the thesis of SUDARSHAN RANGARAJ find it satisfactory and recommend that it be accepted.



Chair



ACKNOWLEDGEMENTS

The author would like to acknowledge the following for their contribution and support in this work:

- Dr. Lloyd Smith, for serving as my advisor and mentor over the past two years. I have had the privilege of working with Dr. Smith as one of his first graduate students, and this has been a very enjoyable learning experience. He has always been a source of knowledge and motivation to me. I wish to thank him for all the support, patience, encouragement and guidance. His insight and wide experience in this field has helped me a lot. I am grateful for the time he has spent with me in discussions. I will always be grateful to him for giving me an opportunity to learn under his guidance.
- Dr. Michael Wolcott, for serving on my committee. He provided useful inputs and suggested improvisations to my work during our research meetings. I am grateful to him for giving me the opportunity to work on this project and be a part of his group, from which I have gained a lot.
- Dr. Tim Adcock and Dr. John Hermanson, for providing me with material for testing and lots of useful information which helped my research and my understanding of wood composites.
- Dr. William Johns, for serving on my committee and his useful suggestions along the way.
- The staff and students at the Wood Materials and Engineering Laboratory for letting me use the equipment and facilities there and for their friendly interaction and prompt help.

- The Wood Materials and Engineering Laboratory - WSU for providing me with funding in the form of research assistantships.
- The School of Mechanical and Materials Engineering - WSU for providing me with funding in the form of a teaching assistantship in the beginning of my graduate program.
- Norman Martell and other staff from the machine shop who helped me deal with problems in the load frames and hydraulic pumps.
- Carmelo Delgado for helping with the SEM pictures.
- This work was supported by the Office of Naval Research and the Wood Materials and Engineering Laboratory at Washington State University, under contract No. 00014-97-C-0395. Their support is gratefully acknowledged.

DURABILITY ASSESSMENT AND MODELING OF WOOD-THERMOPLASTIC COMPOSITES

Abstract

by Sudarshan Rangaraj, M.S.
Washington State University
August 1999

Chair: Lloyd V. Smith

The present work investigates the effects of simulated marine environments on the performance of wood-thermoplastic composites under static and cyclic loading. Durability studies were done for a flat pressed material and two extruded formulations. Moisture sorption studies for these formulations along with dry and wet static test results are presented. The response of the flat pressed material to cyclic loading was investigated by conducting fatigue studies. Sorption induced degradation in properties was observed in the materials studied. During immersed fatigue, the synergistic action of moisture and cyclic loading accelerate damage and lower fatigue life.

Creep studies for the flat pressed material revealed the development of damage and permanent deformation when the creep stress amplitude exceeded a threshold value. The creep response below this threshold was modeled using linear viscoelasticity. The effect of damage was modeled by considering an effective stress. The model also incorporates the observed permanent deformation.

TABLE OF CONTENTS

	Page
ACKNOWLEDGEMENTS.....	iii
ABSTRACT.....	v
LIST OF TABLES.....	ix
LIST OF FIGURES.....	x
CHAPTER	
1. INTRODUCTION.....	1
2. BACKGROUND.....	4
2.1 Durability Issues.....	4
2.2 Materials Studied.....	5
2.3 Literature Review.....	9
2.3.1 Moisture Effects.....	9
2.3.2 Fatigue Response.....	11
2.3.3 Time Dependent Response.....	13
2.4 Objectives.....	15
2.5 Thesis Organization.....	16
3. MOISTURE SORPTION STUDIES.....	18
3.1 Introduction.....	18
3.2 Materials.....	18
3.3 Test Methods and Setup.....	20
3.4 Results.....	21
3.5 Model for the Moisture Diffusion Process.....	22

3.6 Determination of Diffusion Constant.....	24
3.7 Discussion.....	26
3.8 Influence of Temperature on Moisture Diffusion.....	27
3.9 Conclusions.....	29
3.10 References.....	30
4. EFFECTS OF MOISTURE ON MECHANICAL PROPERTIES.....	36
4.1 Introduction.....	36
4.2 Test Setup.....	36
4.3 Results and Discussion.....	37
4.3.1 Effects of Processing Method and Additive.....	37
4.3.2 Effects of Moisture Diffusion.....	39
4.3.3 Qualitative Evidence of Damage.....	40
4.3.4 Effect of Moisture Content on Static Properties.....	41
4.4 Conclusions.....	43
4.5 References.....	44
5. FATIGUE RESPONSE OF THE FLAT PRESSED MATERIAL.....	51
5.1 Introduction.....	51
5.2 Test Setup.....	52
5.3 Results and Discussion.....	53
5.3.1 Influence of Saturation and Immersion on Fatigue Behavior.....	53
5.3.2 Model for Fatigue Life.....	54
5.3.3 Damage Accompanying Fatigue Loading.....	54

5.4 Conclusions.....	56
5.5 References.....	57
6. VISCOELASTIC RESPONSE OF THE FLAT PRESSED MATERIAL.....	62
6.1 Introduction.....	62
6.2 Quasi-Static Tension Tests.....	63
6.3 Creep Characterization Tests.....	63
6.3.1 Test Setup.....	63
6.3.2 Creep Response in the Linear Range.....	65
6.3.3 Non-Linear Response.....	66
6.4 Model Verification Tests.....	71
6.5 Conclusions.....	73
6.6 References.....	74
7. SUMMARY AND FUTURE DIRECTION	87

LIST OF TABLES

2.1 Description of materials included in the study.....	5
2.2. Constituent description and suppliers for flat pressed material.....	6
2.3. Constituent description and suppliers for extruded material.....	8
3.1 Comparison of specific gravities.....	19
4.1 Description of static tests.....	37
4.2 Comparison of static stiffness.....	38
6.1 Creep test matrix.....	64

LIST OF FIGURES

3.1 Moisture diffusion data in distilled water at 30°C.....	32
3.2 Moisture diffusion data in seawater at 30°C.....	32
3.3 Comparison of saturated weight gain.....	33
3.4 Comparison of diffusion constants.....	33
3.5 Comparison of measured diffusion data with a Fickian diffusion model.....	34
3.6 Variation of diffusion constant with temperature.....	35
4.1(a) Comparison of static stiffness.....	45
4.1(b) Comparison of static strength.....	45
4.2 Microscopic surface images of flat pressed coupons.....	46
4.3 Microscopic images of fracture surfaces.....	47
4.4 Microscopic images showing particle matrix interface on the fracture surface.....	48
4.5 Microscopic images showing particle matrix interface on the fracture surface.....	49
4.6 Stiffness and strength reduction during sorption for flat pressed material.....	50
5.1 Fatigue data for flat pressed material.....	58
5.2 Fatigue data for flat pressed material based on percent of ultimate stress.....	59
5.3 Correlation between fatigue life model and data for the flat pressed material.....	60
5.4 Stiffness reduction during fatigue loading.....	61
5.5 Comparison of normalized damage rates for dry and saturated-immersed fatigue tests.....	61
6.1 Quasi-static tension test in the non-linear range.....	75

6.2 Comparison between Eq. (6.3) and a representative coupon in the linear range for creep and recovery.....	76
6.3 Ratio of unloading and loading compliance as a function of creep stress and duration in the non-linear range.....	77
6.4 Permanent strain as a function of creep stresses and duration in the non-linear range.....	78
6.5 Permanent strain as a function of maximum coupon strain.....	79
6.6 Comparison between Eq. (6.6) and damage parameters A and B obtained from best fit data.....	80
6.7 Comparison between Eq. (6.10) and a representative coupon at a creep stress of 5.796 MPa for creep and recovery.....	81
6.8 Comparison between Eq. (6.10) and a representative coupon at a creep stress of 4.692 MPa for creep and recovery.....	82
6.9 Comparison between Eq. (6.15) and a representative coupon for the model verification test with $\sigma_2 > \sigma_1$, creep and recovery for second step.....	83
6.10 Comparison between Eq. (6.16) and a representative coupon for the model verification test with $\sigma_2 < \sigma_1$, creep and recovery for second step.....	84
6.11 Comparison between Eq. (6.16) and a representative coupon for the model verification test with $t_{02} < t_{01}$ and $\sigma_2 = \sigma_1$, creep and recovery for second step.....	85

DEDICATION

This thesis is dedicated to the loving memory of my late mother. Her academic achievements have always been a source of inspiration to me. I owe gratitude to my family for their constant love, encouragement and support.

CHAPTER ONE

INTRODUCTION

Much of the navy's shore facilities established during or following the World War II were constructed using preservative treated wood. These materials are prone to mechanical and biological degradation in their service environments. Due to the age of these structures and the preservative treatment of wood, many problems have arisen in recent years. It is estimated that the navy currently expends \$40-\$50 million annually in replacement, repair and rehabilitation of the degraded lumber products. In addition the material removed presents a disposal problem. Approximately 7000 to 8000 tons of mechanically and/or biologically deteriorated material is removed from service annually. This material being pesticide treated may be hazardous waste and poses large disposal costs. There have also been environmental concerns over water quality from leaching. The decline in availability of timber in the recent past also discourages the use of treated lumber.

New shorefront structures require larger service loads and are more suited to steel or concrete. This has led to the decline in the use of chemically treated wood. However, the navy's current policy has been to develop wood replacement wherever possible.

The degradation of waterfront facilities thus represents an enormous expense in material and maintenance. The need to develop a durable, cost effective and environmentally benign alternative to chemically treated wood clearly exists.

Early wood-polymer composites were designed as direct lumber substitutes. These products do not exhibit particularly high static stiffness and strength and have poor

creep characteristics and fatigue performance. However, these products have greater degradation resistance in comparison with conventional lumber and hence have been quite successful. The objective of this project is to combine the resistance to moisture and bio-degradation of these wood-polymer composites with the increased mechanical performance afforded by other engineering materials. The work presented in the following is a part of the materials development effort aimed at approaching the goal of engineered wood-polymer composites for naval waterfront facilities.

New material formulations and processing methods are being developed to produce these materials cost effectively up to desired performance levels. Durability studies are therefore necessary to model and compare the performance of these candidate materials in their required service environments. The work presented here is a part of the three-year durability modeling program for these engineered wood-polymer composites and is intended to support the activities associated with developing and implementing these new materials. The focus here was to outline appropriate test methods and develop durability models, conduct trial durability studies on a few of the preliminary candidate materials thereby attempting to validate the methods and models. The tests conducted in this study were hence of the "proof of concept" nature. The thesis therefore focuses on these issues rather than detailed statistical data analysis.

Traditional fendering system at a waterfront facility

To get an idea about the intended applications for these materials an overview is presented of the various structural elements that comprise a typical waterfront facility. The components of a traditional fendering system are:

- Vertical fender piles.
- Chocks that separate the piles.
- A wale behind both the chocks and the piles.
- Camels in front of the piles.
- Dolphins as free standing piles.

The fender piles, traditionally made of timber, are vertically driven. These are structural load bearing components and they also exclude debris from getting under docks. The fender piles have most of their length submerged in the water. Chocks connect the individual piles. These are not high load bearing components. Wales are horizontal members running continuously behind the fender piles. They are often made as square 12x12 inch timber sections.

Camels act as floating bumpers between the ships and the fender. These hence have to take up sizeable impact loads. They are secured by connecting chains, this provides longitudinal flexibility. Dolphins are a freestanding timber pile system used to direct ship traffic. They are driven in up to a fixed depth for prescribed flexibility and the piles are fastened with cables.

All of these structural elements have different load bearing requirements and hence can be made from different types of wood-polymer composites. Critical load bearing components may be made from wood-polymer composites reinforced with continuous carbon fibers to enhance stiffness, strength and durability. Less critical components may not require fiber reinforcement and can be comprised of wood, thermoplastic, thermosets and suitable additives.

CHAPTER TWO

BACKGROUND

2.1 Durability Issues

These materials are intended for service under immersed conditions in seawater and will be subjected to seasonal changes in temperature. During installation and service, the material will be subjected to static and dynamic loads arising from pile driving, vessel impact and wave loading under immersed conditions. The loads during pile driving are known to be significantly high. In addition, the material may also experience sustained dead loads from overlying structures or cargo.

Durability studies were hence done under simulated marine conditions. Moisture studies combined with fatigue loading provide a way to simulate and model the service loads and environments on candidate materials. Since these materials contain a significant volume fraction of a polymer matrix, creep may occur at all load levels. Hence the viscoelastic response of the material was characterized and modeled.

Hence the key durability issues considered in this study are:

1. Moisture sorption studies.
2. Effect of prolonged seawater exposure on static strength and stiffness.
3. Fatigue response and effects of moisture on fatigue.
4. Viscoelastic response.

2.2 Materials Studied

2.2.1 Composition

The materials in this study were made from two processing methods: flat pressing and extrusion. These materials consist of wood (maple) flour embedded in a high-density polyethylene (HDPE) matrix. Other components included thermosets (diphenylmethane diisocyanate, M.D.I. and phenol formaldehyde, P.F.) and lubricants (zinc stearate and wax) to enhance flow properties during processing. In addition, an extruded formulation containing talc ($Mg_3Si_4O_{10}(OH)_2$) as an additive was also considered. Constituents in each of the materials investigated and their proportions are summarized in **Table 2.1**.

Table 2.1: Description of materials included in the study (weight % of constituents).

Nomenclature	Process	Wood	HDPE	Thermoset	Lubricants	Talc
Flat pressed	Flat pressing	70%	27%	2% MDI	1%	-
Extruded P.E.	extrusion	65%	27%	2% MDI + 3% P.F.	3%	-
Extruded P.E. + talc	extrusion	55%	27%	2% MDI + 3% P.F.	3%	10%

2.2.2 Processing overview

This section presents a brief overview of the flat-pressing and extrusion processes used to manufacture the materials in this study. A detailed description of the flat-pressing

and extrusion processes may be found in Wolcott, 1998 and Adcock et al., 1999 respectively.

Flat pressing

The flat-pressed panels were manufactured from a Strandex[®] extrusion grade formulation with composition as indicated in **Table 2.1** which includes all the additives typical of an extrusion-grade formulation. Further details of the constituents are provided in **Table 2.2**.

Table 2.2. Constituent description and suppliers for flat-pressed materials.

Component	Description		Supplier
Maple wood flour (40 mesh)	Specific gravity	0.4-0.7 g/cc	American Wood Fibers (4010)
High density polyethylene	Melt temperature	126-135 °C	Equistar (Petrothene – LB 0100)
	Melt flow index	0.40 g/10 min	
	Specific gravity	0.95 g/cc	
	Structure	Crystalline	

Two hundred pounds of the material was mixed at Strandex[®] Corp. in Madison, WI and shipped to the Wood Materials and Engineering Laboratory-WSU, where the panels were manufactured.

An electrically heated, computer automated hot-press was used to manufacture all the panels in this study. The press is equipped with nominal 790 x 585 mm. (31 x 23 inch) platens which are driven by a 200 ton servo-hydraulic system. In general, the press was controlled using platen position with a three-stage press schedule that included: 1) press closing; 2) panel pressing; and 3) venting. A platen temperature of about 180°C was used during panel production. The panels were removed from the hot-press following venting and immediately cooled to ambient temperature under pressure in a cold press.

The press closing time, panel pressing time and venting time were 30 sec, 90 sec and 20 sec respectively for the 3 mm (0.125 in.) thick panels. Panels were formed to a target density by depositing the pre-mixed Strandex[®] formulation into a frame composed of isocyanurate foam building board. The frame is fastened loosely at the corners with staples and serves to contain the furnish during both forming and pressing. All panels were formed and pressed using anodized aluminum caul plates coated with a silicone-based release agent. Complete details of this processing method can be found in Wolcott, M. P., "Flat-Pressing of Strandex Phase I: Processing Parameters", Wood Materials Engineering Laboratory, Washington State University, Pullman WA 99164, and related documents.

Extrusion

The extruded formulations were blended and extruded at the Wood Materials Engineering Lab.-WSU in a twin screw, counter-rotating extruder. The constituents were procured from commercial suppliers. A brief description of the various constituents is given in **Table 2.3**. All the components, other than the wood flour, which was dried to a moisture content of 1%, were used as received from supplier.

Standardized formulations, as listed in **Table 2.1** were prepared and processed in general accordance with the methods outlined by Adcock et al., 1999. The vacuum drawn upon the extruder barrel during WPC manufacture was varied between -28 in. Hg, and -7 in. Hg. The barrel, screw and die temperatures in the extruder were 305, 305 and 320 °F respectively. The die zone temperatures at die entry, central plate and die exit were typically 360, 300 and 300 °F respectively. The screw rotation rate, which directly influenced production rate, was systematically altered between 5 rpm and 20 rpm during

manufacture. Constituents of the extruded formulations were mixed in a drum blender for ten minutes. The material was then extruded into boards 152 mm (6in.) wide and 2.43 m. long. Complete details of the processing method can be found in Adcock, T, Wolcott, M.P., and Hermanson, J.C., 1999, "The influence of wood plastic composite formulation: studies on mechanical and physical properties", Wood Materials and Engineering Laboratory, WSU, Pullman, WA. and related documents.

Table 2.3. Constituent description and suppliers for extruded materials.

Component	Description		Supplier
Maple wood flour (40 mesh)	Specific gravity	0.4-0.7 g/cc	American Wood Fibers (4010)
High density polyethylene	Melt temperature Melt flow index Specific gravity Structure	126-135 °C 0.40 g/10 min 0.95 g/cc Crystalline	Equistar (Petrothene – LB 0100)
MDI	4,4'–diphenylmethane diisocyanate		Bayer Corporation (Mondur 541)
Phenol formaldehyde	Two stage phenolic resin		Plenco Plastics (Plenco 12631)
Zinc stearate	Melt temperature	248-270°F	CDI Inc.
Wax	N,N'–ethylene bisstearamide Melt temperature	284-288°F	GE Specialty Chemicals

2.3 Literature review

2.3.1 Moisture effects

Moisture is known to have a significant effect on polymers and their composites. Unlike metals, polymers absorb moisture from their environment. Further, this absorbed moisture can bring about changes in the mechanical response of the material.

Moisture transport in composites can be modeled using the Fick's law of diffusion, which is the simplest model for diffusion of a solvent into a solid. Three-dimensional anisotropic Fickian diffusion models were developed by C. H. Shen and G. S. Springer, 1981. These models were subsequently verified with moisture sorption data in seawater for graphite-epoxy, glass-epoxy composites (A. C. Loos and G. S. Springer, 1981, Pomies et al., 1995), for jute-epoxy composites (Rao et al., 1988) and for carbon-epoxy (Pomies et al., 1995). These studies consider the effects of fiber volume fraction and fiber orientation (internal factors) on the diffusion constant and equilibrium moisture content.

Another study (Rao et al., 1988) reports the effects of fluid (seawater) temperature and relative humidity of the environment (external factors) on diffusion constants and equilibrium weight gain. A detailed characterization of moisture sorption in epoxy resins was reported by Woo and Piggot, 1987 where the effects of temperature and relative humidity on diffusion constant and activation energy was investigated.

The above studies report that most polymer composites adhere to Fickian behavior, departures from the Fickian response may be associated with material degradation

and moisture-induced plasticization of the polymer matrix. The type of fluid and its temperature can significantly influence diffusion rate and equilibrium weight gain.

Abundant literature exists on moisture sorption in structural wood (Skaar, 1988, Bodig, 1989), such data is also commonly available in structural timber handbooks. Relatively less information exists on moisture sorption in wood-polymer composites immersed in aqueous environments and its impact on mechanical properties. One such study (M. A. Khan and S. Rahman, 1991) reports moisture sorption isotherms for wood plastic composites and compares the moisture resistance of the wood-polymer composite to pure wood of the same species.

Moisture sorption is known to affect the mechanical properties of polymer composites. Many of these studies have been on advanced composites intended for aerospace, automotive and high strength offshore structural applications. Ashbee et al., 1967 studied water damage in polyester resins using optical microscopy, scanning electron microscopy and electron probe X-ray microanalysis. The damage was attributed to osmotic pressure pockets created in the vicinity of water soluble inorganic impurity inclusions.

It has been reported (Tsotsis and Weitsman, 1990 and Ashbee et al., 1967) that in fiber reinforced polymer composites subjected to seawater environments, there is a difference in fluid concentration between the bulk polymer matrix and the particle/fiber-matrix interface. They suggest that this is caused by an osmosis phenomenon, with the polymer serving as a semi-permeable membrane. Further, there also exists, a mismatch between the hygrothermal expansions of the matrix and reinforcement. The combined

influence of these effects may cause fracture of the fiber matrix interfaces and distributed matrix cracking. Which would consequently lead to a degradation in strength and stiffness.

Pomies et al., 1995 reported quantitative (static stiffness and strength data) and qualitative (micrographs) evidence of degradation in polymer composites subjected to marine environments. Seawater induced damage to the fiber matrix interface was reported in this study.

Some of the key issues associated with the mechanical performance of polymer composites in the presence of fluid environments concern their dimensional stability, stiffness and strength. Weight gain at saturation, thickness swell, diffusion rate and impact of marine environments on strength and stiffness should therefore be the important factors considered in evaluating candidate wood-polymer composites intended for the current application.

2.3.2 Fatigue response

A significant amount of literature exists on fatigue damage mechanisms, models for fatigue damage and frameworks for fatigue life diagrams. Though these have focussed around advanced fiber reinforced composites. Many of these concepts can be applied to the material at hand with suitable modifications and assumptions.

Talreja, 1987 provided a review of fatigue damage mechanisms in polymer composites along with a conceptual framework for developing and interpreting fatigue life diagrams for composites. The need for fatigue life diagrams based on the maximum first cycle strain was proposed by Talreja, which is based on the basic mechanisms of

development and growth of fatigue damage. This work also discusses stiffness degradation in composites as a result of fatigue damage.

Constitutive relations for modeling damage in composites have been proposed based on principles of irreversible thermodynamics and continuum mechanics. Ledveze, 1986 developed the mesoscale composite damage theory and showed it to be robust for predicting the damaged response of composites under a wide variety of conditions. It was based on the method of a local state expressed in terms of internal state variables and associated thermodynamic forces. Talreja, 1990 presented an internal variable damage mechanics characterization for orthotropic laminates. Here, damage was characterized by a second order tensor field and constitutive relations were developed for stiffness degradation in damaged laminates.

Fluid environments can have a significant effect on the fatigue response of polymers and polymer composites. Though many investigations have considered fatigue response of saturated coupons in air, fatigue under immersed conditions has received less attention. L. V. Smith and Y. J. Weitsman, 1996 studied the fatigue response of carbon-epoxy cross-ply specimens immersed in seawater. This study showed that during immersed fatigue, water trapped inside cracks caused by fatigue loading can alter the stress state in the coupon, accelerate damage and lower fatigue life.

P. L. Chiou and W. L. Bradley, 1990 studied fatigue damage in graphite-epoxy composites immersed in seawater. This study considered the reduction in stiffness and growth of delamination and provided a correlation between the two effects.

Established frameworks exist for developing fatigue life diagrams and methods are available to characterize fatigue damage in polymer composites. Saturation and

immersion can have a significant influence on fatigue life and damage growth, these effects can be investigated by performing immersed fatigue studies.

2.3.3 Time dependent response

Polymers show inherent time dependent behavior. In composites, the time dependence of the polymeric matrix is accompanied by the temporal behavior of the reinforcements. Time dependent response may be an important issue for the materials at hand since they have a significant volume of a polymer matrix and no continuous reinforcement. Complicated damage mechanisms like interfacial cracking and distributed microcracking can accompany the time dependent response. Though a significant amount of literature reports work on linear viscoelastic response and associated models, relatively less information exists on non-linear viscoelasticity.

A variety of models are available for creep response of polymeric composites. Flugge, 1967 and many such books on viscoelasticity present a review of models that employ series and parallel combinations of springs and dashpots such as the Kelvin-Voigt, Maxwell, Zener model and combination of these. These models have their individual drawbacks and advantages in predicting creep and recovery response.

Jerina et al., 1982 modeled the time dependent compliance using a power law expression and showed that the strain response of the viscoelastic material to a step stress input was given by a relatively simple expression. The parameters in this expression are material constants that can be easily determined from the creep and recovery data. As observed by many workers, the time dependent response of many polymeric materials and their composites can be satisfactorily described using this power law model.

L. V. Smith and Y. J. Weitsman, 1996 presented creep studies on swirl-mat composites using the power law compliance. They incorporated the effects of distributed continuum damage and permanent deformation into the power law model using the concept of effective stress (Lemaitre and Chaboche, 1990). In subsequent work, the same authors (L. V. Smith and Y. J. Weitsman, 1998) investigated the development of damage in swirl mat composites under repeated ramp loads. Damage, as a function of load cycle, was incorporated into the non-linear model developed for creep/recovery response.

Chia et al., 1986 modeled creep in a wood-polymer composite using a power law model in which creep strain was expressed as a function of time, applied stress level and temperature. Their model correlated well with data for linear viscoelastic response but cannot incorporate effects of damage and plastic strains in an elegant manner. Further, determining the constants in the model involved rigorous statistical analysis.

The power law expression proposed by Jerina et al., 1982 may be used to model the viscoelastic response of the material at hand. Effects like damage and viscoplasticity may then be incorporated into the viscoelastic framework quite easily. In the event that this power law model is unable to adequately represent the observed response, more complicated models incorporating combinations of springs and dashpots can be employed.

The influence of moisture on creep response may be modeled using a time-moisture superposition principle as discussed by Maksimov et al., 1972. The effect of moisture is modeled by considering the contraction of time scales using a moisture shift factor.

P. C. Upadhyay and A. Mishra, 1994 developed a generalized parametric model for moisture assisted creep in a polymeric composite. They described the effects of moisture on creep compliance and strain using non-dimensional parameters, these results were hence in a generalized form and may be applicable to a wide range of composites.

2.4 Objectives

The main objective of this work is to characterize fluid sorption and determine its effects on mechanical properties of the wood-polymer composites when exposed to aqueous environments. Hence, from the review of durability literature, the detailed objectives of this research can be outlined as:

1. Moisture sorption studies

- Study moisture diffusion in the material in seawater and distilled water.
- Model the moisture diffusion process and determine diffusion constants.
- Study the influence of temperature on diffusion.
- Investigate the effects of moisture diffusion on strength and stiffness.

2. Fatigue response

- Establish and model fatigue life data for the material.
- Study and model damage accompanying fatigue loading.
- Investigate the effects of saturation and immersion on fatigue life and damage growth.

3. Viscoelastic response

- Characterize linear viscoelastic response from creep and recovery tests.
- Quantify non-linear effects such as damage and permanent deformation.
- Develop a predictive model for viscoelastic response incorporating these effects.
- Verify the correlation between the data and model predictions.
- Validate the model through verification tests.

2.5 Thesis organization

In the following, results and discussions of tests conducted according to the outlined objectives are presented. Details of the relevant test methods, experimental procedures and conclusions are incorporated within individual chapters.

Chap. 3 covers the moisture sorption studies. Moisture sorption data for the three materials investigated are presented along with correlations between the diffusion data and a linear Fickian diffusion model. Temperature effects on diffusion are studied. Effects of prolonged seawater exposure on static strength and stiffness are examined in **Chap. 4**. These effects are quantified from changes in stiffness and strength and qualitatively analyzed.

Chap. 5 deals with the fatigue response of the flat pressed material. Effects of moisture on fatigue response are studied by performing immersed fatigue tests of dry and saturated coupons. Damage accompanying fatigue loading is quantified from modulus softening data. Individual effects of moisture sorption, capillary action and fatigue loading are explained.

Chap. 6 discusses the viscoelastic response of the flat pressed material along with the observed features of damage and viscoplasticity. A model for viscolastic response is developed that incorporates the observed effects of viscoplasticity and damage. Correlations between the model and test data are presented from creep characterization tests as well as verification tests.

A summary is presented and recommendations for this work are sighted in **Chap. 7**. Future directions to the project based in findings from this study are also suggested.

CHAPTER THREE

MOISTURE SORPTION STUDIES

3.1. Introduction

To understand the combined effects of moisture, fatigue and creep, their individual contributions must first be understood. Accordingly, moisture sorption studies were performed to compare the moisture diffusion process in three candidate materials. The effects of internal variables (additives and processing methods) and external variables (fluid environment and temperature) on the diffusion process are examined. Damage due to moisture sorption was assessed by measuring the coupon stiffness and strength during and after saturation.

In the following, a study of the moisture diffusion process is presented along with correlations between the diffusion data and a Fickian diffusion model. Qualitative evidence of moisture induced damage is presented and correlated with observed changes in mechanical performance.

3.2 Materials

Moisture sorption studies were performed for the three materials described in Table 2.1. The specific gravity of these three materials was estimated by measuring the weights and volumes of the coupons. The average specific gravity for each of these materials is summarized in Table 3.1. These measured values are compared with the predictions of the rule of mixtures (ROM) which considered the individual densities and volume fractions of the wood particles and matrix. The HDPE, thermosets and lubricants

were accounted for as a single matrix phase. The specific gravity of the wood flour, matrix and talc were taken to be 0.70, 1.20 and 2.65 respectively.

Table 3.1: Comparison of specific gravitates

Material	Component	Mass fraction	Volume fraction	ROM prediction of composite sp. grav.	Measured composite sp. grav.
Flat pressed	Wood	0.7	0.747	0.95	0.95
	Matrix	0.3	0.252		
	Talc	0	0		
Extruded P.E.	Wood	0.65	0.720	0.96	1.01
	Matrix	0.35	0.279		
	Talc	0	0		
Extruded P.E. + talc	Wood	0.55	0.658	1.04	1.06
	Matrix	0.35	0.302		
	Talc	0.10	0.039		

As seen in Table 3.1 that the ROM yields a lower estimate of specific gravity in comparison with the measured values for all the three materials. This is probably because the ROM calculation does not account for the compaction of the individual constituents taking place during flat pressing and extrusion causing an increase in their specific gravity. Also, the specific gravity of solid wood was used in the calculations, the specific gravity of wood in fine particulate form may be higher than 0.7. Another reason for error may be that the void volume is not accounted for in these calculations.

However, the ROM predictions are intended to give a comparative estimate of the effects of the individual constituents on the density of the composite. The measured specific gravity values give a relative estimate of the degree of compaction achieved in the two processing methods. This may influence moisture sorption, strength and stiffness.

3.3 Test methods and setup

Flat pressed coupons 210 mm (8 in.) long and 25 mm (1 in.) wide were cut from 305 mm x 305 mm panels, 3mm (0.125 in.) thick. A periphery of 25 mm (1in.) was trimmed of from the panel edges. The extruded coupons 210 mm (8 in.) long and 25 mm (1 in.) wide were cut from extruded boards 610 mm long, 152 mm wide and 6 mm thick. A similar trimming operation was used for the extruded boards as well. All cutting operations were performed on a table saw equipped with a rotating cutting blade and stops for controlling the width of the cut.

These coupons were then immersed in temperature controlled (30°C) water baths containing seawater or distilled water. These water baths had a temperature range of 10°C to 90°C and a controlled bath temperature to $\pm 3^\circ\text{C}$ of the desired temperature. The dimensions of the water baths were 508 mm (length) x 305 mm (width) x 152 mm (depth). Simulated seawater was obtained by mixing Instant Ocean[®] with distilled water to obtain a specific gravity of 1.022 that is typical of ocean water. The coupons were placed horizontally on their faces (1 x 8 in.) in the water bath with a 2-3 inch depth of immersion. Coupons were periodically removed from the bath, wiped with a dry cloth and measured on a Sartorius-BP 211D analytical balance to the accuracy of 0.01 milligram. When the coupons are being

weighed some moisture is lost by evaporation from their surface. However, these losses did not exceed 1 milligram. The weight measurements were hence accurate upto 1 milligram.

3.4 Results

It may be useful to introduce some of the terms encountered in the following discussions. The percent weight gain (%M) is given by

$$\%M = \left(\frac{M_{\text{wet}} - M_{\text{dry}}}{M_{\text{dry}}} \right) \cdot 100 \quad (3.1)$$

where M_{wet} is the weight of the wet coupons (immersed in the water bath) and M_{dry} is the coupon weight in the "as processed" condition before it is put into the water bath. The moisture concentration in the coupon (m) is given by

$$m = \frac{(M(t) - M_{\text{dry}})}{(M_{\text{sat}} - M_{\text{dry}})} \quad (3.2)$$

where $M(t)$ and M_{sat} are the total weight of an immersed coupon at any given time and at saturation respectively. Further, the moisture content per unit dry weight of the coupon (c) is defined as

$$c = \frac{M_{\text{wet}} - M_{\text{dry}}}{M_{\text{dry}}} \quad (3.3)$$

Moisture weight gain (%M) is plotted as a function of time for the three materials (flat pressed, extruded P.E. and extruded P.E. + talc) in distilled water at 30°C in **Fig. 3.1**, and in seawater at 30°C in **Fig. 3.2**. When the percent weight gain of the coupons is plotted

against the square root of time (**Figs. 3.1 and 3.2**) an initial linear region is observed, followed by a curvilinear region where the coupons asymptotically approach saturation. This pattern of moisture related weight gain resembles that predicted by Fick's Law of diffusion. A summary of the average weight gain at saturation for the three materials is shown in **Fig. 3.3**.

3.5 Model for the moisture diffusion process

Figs. 3.1 and 3.2 suggest that the moisture diffusion process for the materials at hand follow Fick's law. According to Fick's Law of diffusion (Springer, 1988) the fluid flux, F , is proportional to the concentration gradient, ∇m , or

$$F = -D \nabla m \quad (3.4)$$

Where, D is the diffusion constant. Fluid flux is taken as positive outward, hence we have negative flux for an increasing concentration gradient. Test coupons tend to be thin and flat, where the moisture transport may be approximated as one-dimensional. Considering the conservation of mass for one-dimensional moisture transport we have

$$\partial m / \partial t = -\partial F / \partial x \quad (3.5)$$

Where the negative sign is again due to the outward positive sense of the flux. Combining Eqs. (3.4) and (3.5) gives the governing partial differential equation for one-dimensional Fickian moisture transport, or

$$\partial m / \partial t = D \partial^2 m / \partial x^2 \quad (3.6)$$

Eq. (3.6) can be solved with appropriate initial conditions (IC) and boundary conditions (BC) given as

$$\text{IC} : m(x,0) = m_i$$

$$\text{BC} : m(0,t) = m(h,t) = m_a \quad t > 0 \quad (3.7)$$

Where m_i is the initial fluid concentration in the coupon, and m_a is the constant fluid concentration at the free surface of the coupon, taken to be the saturation value. Following established procedures (Gopalan et al., 1988, Springer, 1988) Eq. (3.6) may be solved as a series solution for moisture concentration in the coupon as

$$\frac{m(x,t) - m_i}{m_{\text{sat}} - m_i} = 1 - \sum_{j=0}^{\infty} \frac{4}{\pi} \cdot \left[\frac{1}{(2j+1)} \cdot \sin \left[\frac{(2j+1) \cdot \pi \cdot x}{h} \right] \right] \cdot \exp \left[\frac{-(2j+1)^2 \cdot \pi^2 \cdot D \cdot t}{h^2} \right] \quad (3.8)$$

In Eq. (3.8) m_i and m_{sat} are the initial (as processed) and saturation values of fluid concentration in the coupon respectively and h is the coupon thickness. In the above solution (Eq. (3.8)) it was further assumed that the coupon free surface concentration, m_a , is the saturation value. The total mass of moisture in the coupon is found by integrating Eq. (3.8) over the volume of the coupon, as

$$M = \int m(x, t) dV = A \cdot \int_0^h m(x, t) dx \quad (3.9)$$

Since for one-dimensional diffusion $dV=A \cdot dx$, where A is the area of the coupon face normal to the direction of moisture diffusion and h is the coupon thickness.

3.6 Determination of diffusion constant (D)

The relative rates of moisture sorption for the three materials were considered by comparing their respective diffusion constants. For a thin (thickness \ll width) and long (thickness \ll length) coupon, diffusion is essentially one-dimensional. According to Fick's law, the percent weight gain, $\%M$, initially varies linearly with the square root of time, t , (Springer, 1988) as

$$\%M = \frac{4 \cdot (\%M_{\text{sat}}) \cdot \sqrt{D_A}}{h \cdot \sqrt{\pi}} \cdot \sqrt{t} \quad (3.10 a)$$

where, $\%M_{\text{sat}}$ is the percent weight gain at saturation, D_A is the apparent diffusion constant and h is the coupon thickness. The apparent diffusion constant D_A may be determined from the slope of this linear region (Springer, 1988) as

$$D_A = \pi \cdot \left[\frac{h^2}{16 \cdot (\%M_{\text{sat}})^2} \right] \cdot \left[\frac{(\%M_2 - \%M_1)^2}{\sqrt{t_2} - \sqrt{t_1}} \right]^2 \quad (3.10 b)$$

$\%M_2$ and $\%M_1$ are coupon percent weight gains at time t_2 and t_1 respectively. Since the apparent diffusion constant given by Eq. (3.10b) is one-dimensional, it does not account for

the diffusion taking place through the coupon edges. This can be accounted for by using a geometric edge correction factor (ECF) that is given by (Rao et al., 1988)

$$ECF = \left(1 + \frac{h}{L} + \frac{h}{w}\right)^2 \quad (3.11)$$

Where h, w and L are the coupon thickness, width and length respectively. Hence the corrected diffusion constant is given by

$$D = \frac{D_A}{ECF} \quad (3.12)$$

The particle size of the wood flour is small, much less than the coupon thickness. The volume fraction of the polymer (HDPE) matrix is sufficiently high (25%), hence there may be a sufficient bulk of the polymer matrix between the dispersed wood particles. As an approximation, isotropic diffusion behavior was assumed. Hence, a one-dimensional diffusion model was used, and diffusion through the edges was accounted for by using the edge correction factor. A more rigorous analysis may entail a consideration of the orthotropic nature of wood, and an exploration of a three-dimensional model with different diffusion rates in the three material directions. For the purpose of comparing materials, as here, this model may be adequate. Moreover, its predictions correlate reasonably well with measured data (**Fig. 3.5**). The average diffusion constants for the three materials (found using Eq. (3.12)) in the two fluid environments (seawater and distilled water) are shown in **Fig. 3.4**.

3.7 Discussion

Predictions of the Fickian model developed earlier (Eq. (3.8)) are compared with the measured weight gain data in **Fig. 3.5** for the flat pressed and extruded materials. In **Fig. 3.5**, the moisture concentration (m) is plotted as a function of non-dimensional time (t_{nd}), given by

$$t_{nd} = \left(\frac{D \cdot t}{h^2} \right)^{0.5} \quad (3.13)$$

As seen from **Fig. 3.5**, the one-dimensional Fickian model, with the correction for edge effects, represents the measured weight gain data reasonably well. Departures from the Fickian model may be associated with material degradation or moisture induced plasticization of the polymer matrix. The Fickian response of the material suggests the absence of such effects. The favorable agreement with Fick's law is not intended to imply that moisture transport occurs only by diffusion. Rather, the diffusion constant determined by this method should be viewed as capturing all moisture transport mechanisms including capillary action due to voids spaces and wood particles.

While the diffusion process appears to be Fickian in all cases, the weight gain at saturation and the diffusion rates are lower in seawater than in distilled water. This may be explained by considering the ionic content of seawater, which can suppress the moisture transport process. This has also been observed in synthetic composites (Gopalan et al., 1988). In general, the extruded materials had lower weight gain at saturation as compared to the flat pressed material. The enhanced consolidation achieved in extrusion, reduces void content and achieves better dispersion of the wood flour in the thermoplastic matrix.

Further, a possible selective orientation may be imparted to the wood particles during extrusion.

Also, the content of wood flour is less in the extruded material as compared to the flat pressed material (flat pressed, extruded P.E. and extruded P.E. + talc contain 70%, 65% and 55% of wood flour respectively). It may therefore be likely that the direct exposure of wood flour to moisture is lower in the extruded materials since they contain a higher fraction of polymer.

These may be some of the reasons for the enhanced moisture resistance of the extruded formulations. The talc additive apparently acts to further reduce saturation weight gain and diffusion rate. Talc is waxlike or pearly in its natural form and is known to have a distinctly greasy feel, which may impart low moisture admittance.

3.8 Influence of temperature on moisture diffusion

When considering service applications, it is helpful to study the effect of temperature on the moisture diffusion process. Accordingly, coupons were immersed in seawater baths at three different temperatures (15°C, 30°C and 45°C) and periodic weight measurements were made as described earlier (3.3). The relation between the diffusion constant and temperature is commonly represented by an Arrhenius type relation (Springer, 1988)

$$D = D_0 \cdot \exp\left(\frac{-E_A}{R \cdot T}\right) \quad (3.14)$$

Where, D_0 is a constant that depends on the coupon material and the fluid environment, E_A is the activation energy, R is the universal gas constant and T is the

absolute temperature. **Fig. 3.6** shows the influence of temperature on the diffusion constant for the flat pressed material. D_0 and E_A are determined from the intercept and slope of the best-fit straight line on a log-log plot of Eq. (3.14) as $D_0 = 11.6 \times 10^{-5} \text{ mm}^2/\text{sec.}$ and $E_A/R = 955.6 \text{ }^\circ\text{K}$ respectively. Eq. (3.14) may be useful in accelerating the saturation of coupons for experimental study, since the weight gain at saturation was not noticeably affected by change in the bath temperature.

3.9 Conclusions

Moisture sorption studies indicate that processing methods and additives can have a significant influence on the moisture diffusion process. A one-dimensional Fickian model represents the diffusion process adequately well for the materials studied. The enhanced consolidation achieved in the extrusion process, imparted improved static stiffness and strength as compared to flat pressing, this effect was further improved by the addition of talc. Fluid temperature had a significant influence on the moisture diffusion rate but did not have a noticeable effect on the saturation weight gain.

3.10 References

- 3.1] Touloukian, Y. S., Judd, W. R., and Roy, R. F., "Physical Properties of Rocks and Minerals," *McGraw-Hill/Cindas Data Series on Material Properties*, II-2, 1981.
- 3.2] Springer, G. S., "Environmental Effects," *Environmental Effects on Composite Materials*, 3: 1-34, 1988.
- 3.3] Springer, G. S., and Shen, C. H., "Moisture Absorption and Desorption of Composite Materials," *Environmental Effects on Composite Materials*, 3: 15-33, 1988.
- 3.4] Loos, A. C., and Springer, G. S., "Moisture Absorption of Graphite-Epoxy Composition Immersed in Liquids and Humid Air," *Environmental Effects on Composite Materials*, 3: 34-49, 1988.
- 3.5] Gopalan, R., Rao, R. M., Murthy, M. V., and Dattaguru, B., "Diffusion Studies on Advanced Fiber Hybrid Composites," *Environmental Effects on Composite Materials*, 3: 96-105, 1988.
- 3.6] Rao, R. M., Balasubramanian, N. and Chanda, M., "Factors Affecting Moisture Absorption in Polymer Composites, Part-1: Influence of Internal Factors," *Environmental Effects on Composite Materials*, 3: 75-87, 1988.
- 3.7] Rao, R. M., Balasubramanian, N. and Chanda, M., "Factors Affecting Moisture Absorption in Polymer Composites, Part-2: Influence of External Factors," *Environmental Effects on Composite Materials*, 3: 89-95, 1988.
- 3.8] Khan, M. A., and Rahman, S., "Moisture Sorption Isotherms of Wood and Wood-polymer Composites," *Polymer-Plastics Technology and Engineering*, 30(5 & 6): 435-440, 1991.
- 3.9] Skaar, C., "Wood-Water Relations," *Springer-Verlag*, 1988.

3.10] Ashbee, K. H. G., Frank, F. C., and Wyatt, R. C., "Water Damage in Polyester Resins," *Proceedings of Royal Society, A* 300: 415-419, 1967.

3.11] Ashbee, K. H. G., and Wyatt, R. C., "Water Damage in Glass Fiber/Resin Composites," *Proceedings of Royal Society, A* 312: 553-564, 1969.

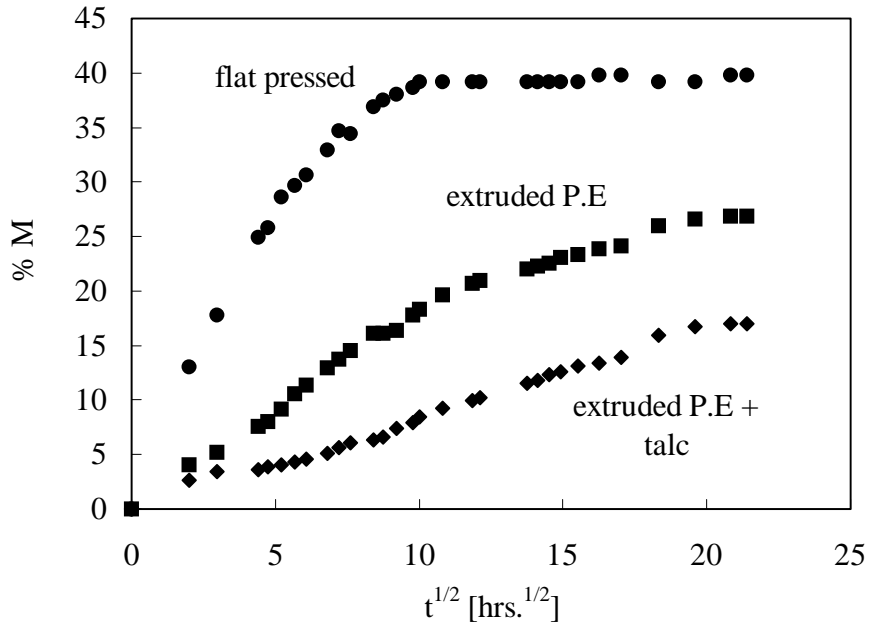


Fig. 3.1: Moisture diffusion data in distilled water at 30°C

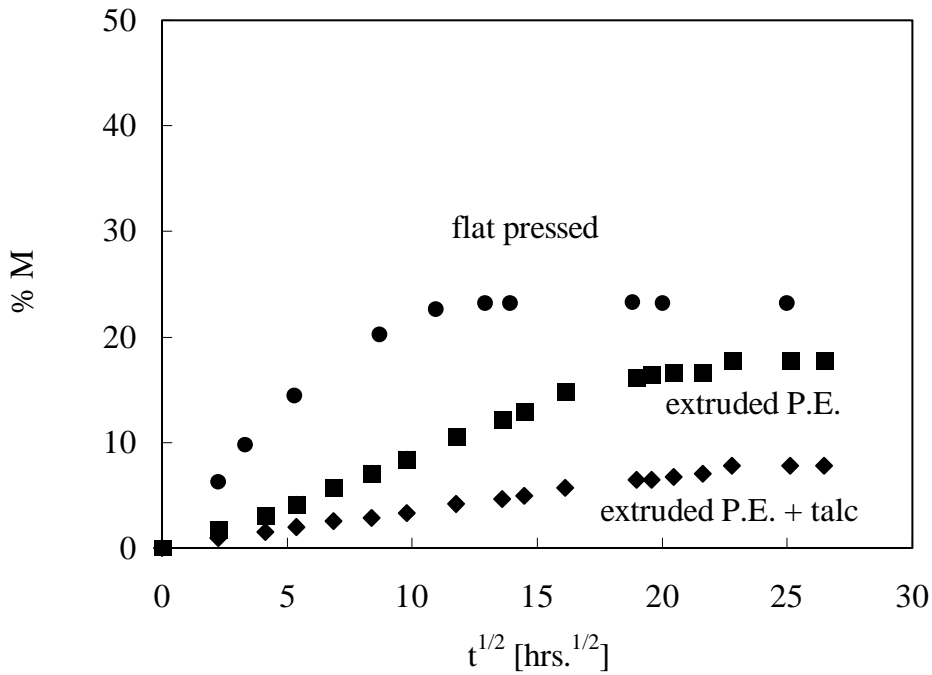


Fig. 3.2 Moisture diffusion data in seawater at 30°C

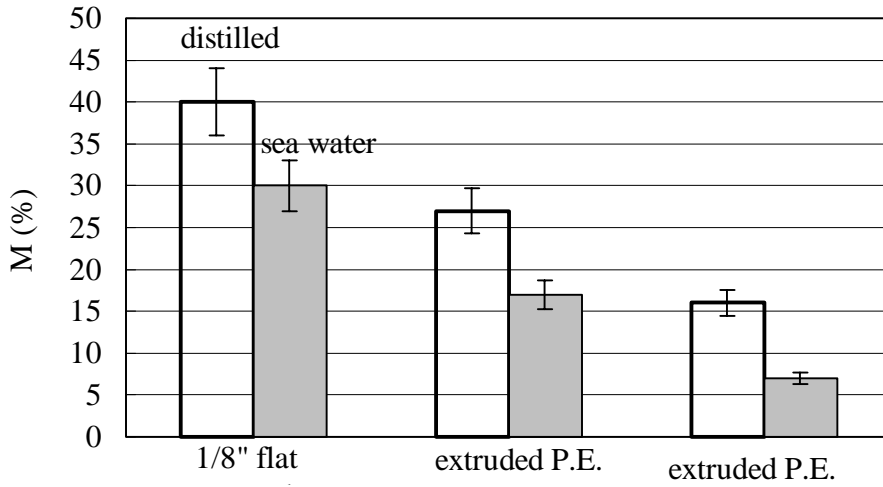


Fig. 3.3: Comparison of saturated weight gain (average values and scatter band)

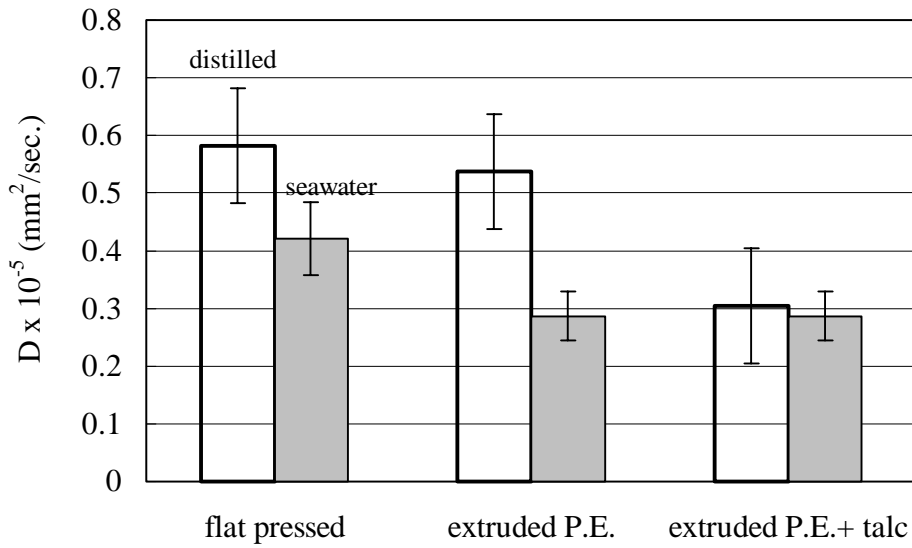


Fig. 3.4: Comparison of diffusion constants (average values and scatter band)

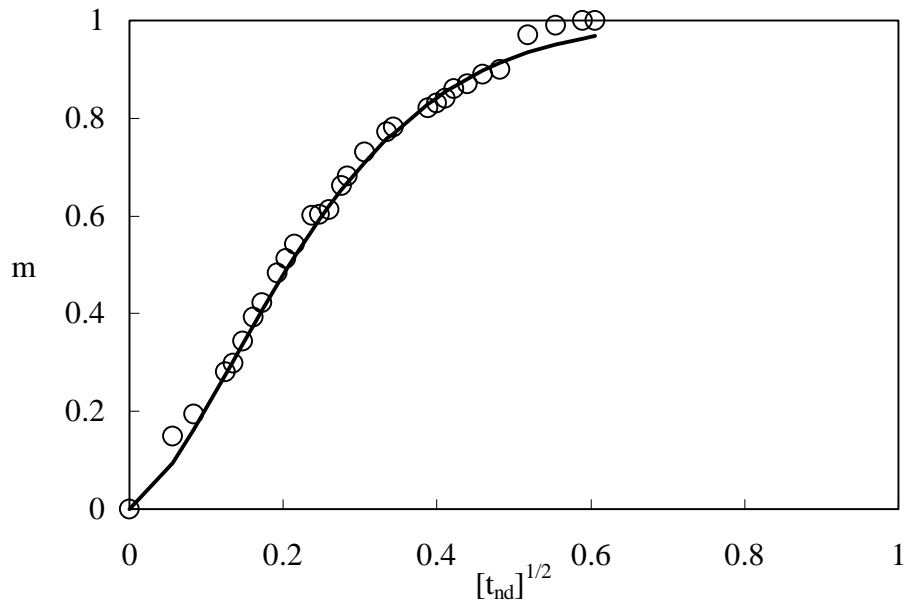
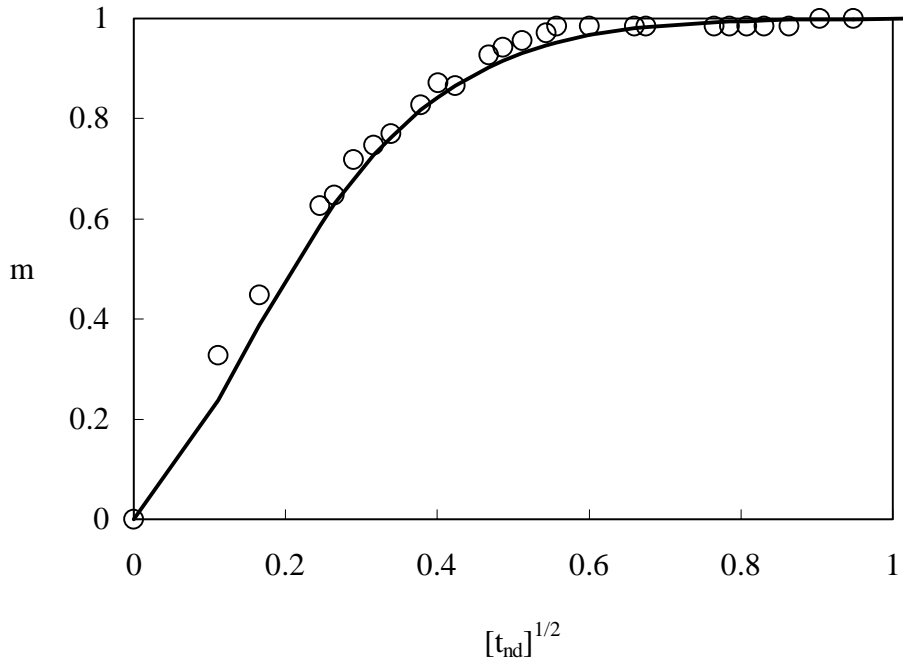


Fig. 3.5: Comparison of measured diffusion data with a Fickian diffusion model for the flat pressed material (top) and extruded P.E. (bottom).

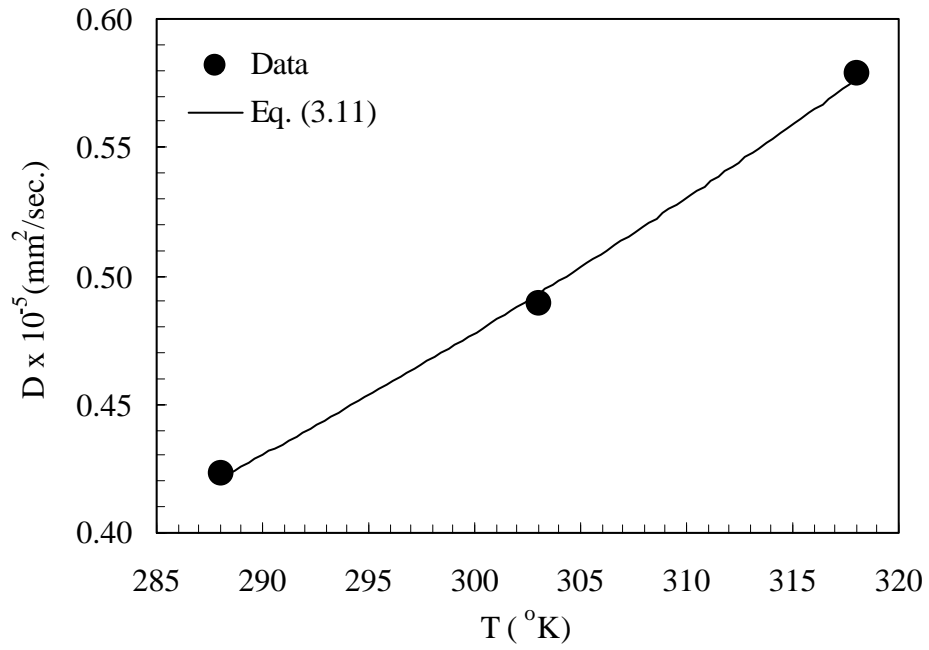


Fig. 3.6: Variation of diffusion constant with temperature

CHAPTER FOUR

EFFECTS OF MOISTURE ON MECHANICAL PROPERTIES

4.1 Introduction

Dry static tests were performed to evaluate the effect of the processing method and additives on static strength and stiffness and evaluate the variability in the material. The materials included in this study were the same as those in the moisture sorption studies. Exposure to fluid environments is known to degrade stiffness and strength in composites (Frederic et al., 1993). Static testing of saturated coupons (wet static tests) were performed to quantify degradation, and measure residual properties after prolonged moisture exposure.

4.2 Test setup

The three types of quasi-static uniaxial tension tests described in **Table 4.1** were done using the guidelines prescribed in ASTM D3039. Coupon geometry and cutting operations were similar to that used for the moisture sorption studies (3.3). The tests were performed on a 4 post 44 kN (20 kip) servohydraulic load frame with mechanical grips. The tests were done in displacement control at a rate of 1.27 mm/min. (0.05 in./min.). Load, actuator displacement and coupon strain were recorded using a computer data acquisition system. Labview software was used for data acquisition. Strains were measured using an extensometer clipped to the coupon surface and a Vishay 2110A signal conditioner. Coupon stiffness was measured as a chord modulus in the linear range of the stress-strain curve.

Table 4.1: Description of static tests

Type of static test	Description	Objectives
Dry static	dry coupons	evaluate effects of processing method and additives on strength and stiffness
Wet static	saturated coupons tested immediately after removal from the water bath	quantify sorption induced damage by measuring loss of stiffness and strength
Dried static	saturated coupons, dried in air at room temp prior to testing	determine if the effects of fluid exposure are permanent and associated with weight loss

4.3 Results and discussion

4.3.1 Effect of processing method and additive

Results from the dry and wet static tests are summarized in **Fig. 4.1**. Extruded coupons were stiffer and stronger than the flat pressed coupons. This can be attributed to the enhanced consolidation achieved in extrusion that is reflected from the higher (5-10%) specific gravity of extruded material (Table 3.1) and the possible selective orientation that may be imparted to the wood-flour particles during extrusion.

Addition of talc into the extruded formulation further enhances strength and stiffness in the dry condition. Talc in its pure mineral form (silicates of magnesium) has a stiffness (secant modulus) of about 33 GPa (4.78 Msi) and strength of 1200 MPa (174 ksi)

(Touloukian et al., 1981). The changes in stiffness appear to be proportional to the volume fraction of the constituents. Using the rule of mixtures (ROM), for instance, predicts a composite modulus of 2.13 GPa (310 ksi) for the flat pressed P.E., 2.31 GPa (335 ksi) for the extruded P.E. and 3.17 GPa (461 ksi) for the extruded P.E. + talc formulation. Measured stiffness values and predictions from ROM are compared in Table 4.2 below. In the ROM calculations the static stiffness of wood flour, matrix (HDPE + thermosets + lubricants) and talc were taken as 2.1 Gpa (305 ksi), 2.76 GPa (400 ksi) and 33 GPa (4.78 Msi) respectively.

Table 4.2: Comparison of static stiffness.

Material	Component	Mass fraction	Volume fraction	ROM prediction of composite Stiffness (GPa)	Measured composite Stiffness (GPa)
Flat pressed	Wood	0.7	0.747	2.13	2.12
	Matrix	0.3	0.252		
	Talc	0	0		
Extruded P.E.	Wood	0.65	0.72	2.31	2.58
	Matrix	0.35	0.28		
	Talc	0	0		
Extruded P.E. + talc	Wood	0.55	0.658	3.17	3.25
	Matrix	0.35	0.302		
	Talc	0.10	0.039		

The measured values seem to follow the ROM predictions quite closely. There is a discrepancy between the measured and predicted values because the estimate of wood flour stiffness may not be accurate and is difficult to make. The ROM predictions are however intended to bring out the relative effects of the constituents and an appreciation for the role of each.

4.3.2 Effects of moisture diffusion

The effect of moisture was significant, where a reduction in strength of around 30% and a reduction in stiffness of about 40% at saturation were typical. The improved stiffness and strength afforded by talc in the dry tests seemed to diminish with moisture sorption however. A 35% reduction in strength and 50% in stiffness at 20-30% weight gain are typical for conventional lumber (Skaar, 1988 and Madsen, 1992).

A group of saturated coupons were dried at either 100°C in an oven or at room temperature to determine if the sorption induced damage was reversible. These were then quasi-statically tested to failure. The strength and stiffness from these tests were similar to the undried saturated results, demonstrating that the effects of moisture were permanent.

The combination of permanent moisture related damage and linear Fickian response can possibly be related to the properties of the composite constituents. A mismatch exists between the hygroscopic expansions of the wood particles and the HDPE matrix. Typically, wood has a hygroscopic expansion coefficient of 0.5-0.7 ϵ/c (Madsen, 1992), where c is the moisture absorbed per unit dry weight of coupon. Additionally wood is known to absorb approximately 25 - 40 % moisture ($c = 0.45$) at saturation. Further, the wood-flour particles were dried prior to processing, this may increase their tendency to absorb moisture when the

coupons are immersed. Whereas, HDPE is known to be relatively unaffected by moisture.

Also, the chemical composition of the wood particle-matrix interface is unlike that of the bulk polymer (HDPE) matrix. It has been reported in earlier work (Ashbee et al., 1967, Ashbee and Wyatt., 1969) that in polymer composites subjected to seawater environments, there is a difference in fluid concentration between the bulk polymer matrix and the particle/fiber-matrix interface. This is caused by an osmosis phenomenon, with the polymer serving as a semi-permeable membrane.

A combination of the above effects may be possibly related to the observed loss in properties. Concrete evidence of the mechanisms controlling stiffness and strength loss due to moisture sorption are unavailable at this point and further studies to verify these hypotheses are required.

4.3.3 Qualitative evidence of damage

Some preliminary attempts were made at qualitatively investigating the effects of moisture sorption using scanning electron microscopy. Prior to these studies the coupons had to be cut to a length of 1 inch, and oven dried for 2-3 hours at 80-100 °C to eliminate moisture present in the material. Subsequently the samples were gold-layer coated in an argon environment using a Hummer VII sputtering system (Anatech Ltd.) to minimize air trapped in voids. A JSM-6400 scanning electron microscope (JEOL Ltd.) was used for this study.

Microscopic images of coupons subjected to these fluid environments for extended time periods (twice the saturation period) reveal differences between dry and saturated coupons. **Fig. 4.2** compares the surfaces of a dry and a saturated flat pressed coupon as seen

under a scanning electron microscope. The surface of the dry coupon appears smooth, except for minute ridges that may be left by processing, whereas the surface of the saturated coupon appears undulating. This may be a result of swelling of wood particles caused by seawater making distinct wood particles visible.

Microscopic images of fracture surfaces on dry and saturated extruded P.E. coupons are compared in **Fig. 4.3**. The fracture surface on the dry coupon appears relatively smooth. The rough appearance of the fracture surface on the saturated coupon may probably be due to the effects of disparate moisture swelling of wood and HDPE and the tendency of wood to regain moisture lost prior to and during processing. Images of higher magnification showing an individual wood flour particle and the surrounding matrix are presented in **Figs. 4.4** and **4.5**, for dry and saturated coupons.

Analysis of these images is complicated by processing (such as gold coating) necessary for SEM imaging and presence of voids. These may modify surface textures on the coupon and create artificial effects. Conclusive evidence to explain a mechanism for moisture induced damage is still unavailable at this point, the above observation methods are still being refined. Attempting a better understanding of the micro-structural internal deformation mechanisms in the wood and matrix due to moisture swelling may be a suitable avenue to further these studies.

4.3.4 Effect of moisture content on static properties

The rate of moisture related degradation was studied by testing coupons with different moisture contents. The coupons were randomly divided into 6 groups, each containing 5 coupons. Each group of coupons was removed from the water bath (30°C) at

the end of a predetermined duration for that group, the coupons were immediately wiped with a dry cloth and weighed to note the percent weight gain (%M). Subsequently, these were quasi-statically tension tested in air following procedures described earlier (4.2). Ratios of the stiffness and strength of wet coupons to the respective dry values are plotted as a function of moisture content in **Fig. 4.6**.

Coupon strength and stiffness loss seems proportional to moisture content up to 50% of the saturation weight gain. At 50% of the saturation weight gain, the stiffness and strength degradation reach steady state. It is recognized that prior to saturation the distribution of moisture may be non-uniform through the coupon thickness and localized closer to the surfaces. This shortcoming may be remedied by enclosing the coupons in a tight plastic bag and allowing sufficient time for the moisture to equilibrate through the thickness

4.4 Conclusions

This study revealed that extruded material has higher stiffness and strength in comparison with the flat pressed material. Incorporation of talc into the extruded formulation can enhance this effect. These effects may probably be attributed to the higher degree of compaction and possible selective orientation of wood-flour particles achieved in extrusion.

Sorption related permanent loss of strength and stiffness at saturation were observed in the materials investigated. The degradation in stiffness and strength were proportional to the moisture content up to a certain level (**Fig. 4.6**). The moisture related degradation may be related to the incompatible moisture expansion of the constituents, tendency of wood to regain moisture lost during processing and osmotic effects. Further study is needed, however, to establish their relative significance. The enhanced strength and stiffness imparted by talc in the dry condition, seemed to diminish with moisture sorption.

4.5 References

- 4.1] Frederic, P., Leif, A. C., and John, W., Gillespie, Jr., "Marine Environmental Effects on Polymer Matrix Composites," *Composite Materials: Fatigue and Fracture, ASTM STP 1230*, Martin, R. H., Ed., American Society for Testing and Materials, Philadelphia, 5: 283-303, 1993.
- 4.2] American Society for Testing of materials, "Standard Test Method for Tensile Properties of Polymer Matrix Composite Materials," *ASTM D 3039/D 3039 M-93*: 118-127, 1993.
- 4.3] Touloukian, Y. S., Judd, W. R., and Roy, R. F., "Physical Properties of Rocks and Minerals," *McGraw-Hill/Cindas Data Series on Material Properties*, II-2, 1981.
- 4.4] Skaar, C., "Wood-Water Relations," *Springer-Verlag*, 1988.
- 4.5] Madsen, B., "Structural Behavior of Timber," *Timber Engineering Ltd.*, 1992.
- 4.6] Gibson, R., F., "Principles of Composite Material Mechanics," Mc Graw Inc, 1994.
- 4.7] Ashbee, K. H. G., Frank, F. C., and Wyatt, R. C., "Water Damage in Polyester Resins," *Proceedings of Royal Society*, A 300: 415-419, 1967.
- 4.8] Ashbee, K. H. G., and Wyatt, R. C., "Water Damage in Glass Fiber/Resin Composites," *Proceedings of Royal Society*, A 312: 553-564, 1969.
- 4.9] Rangaraj, S. V., and Smith, L. V., "Moisture Effects on Durability of a Wood-Thermoplastic Composite," – in review, *Journal of Thermoplastic Composite Materials*.
- 4.10] Rangaraj, S. V., and Smith, L. V., "Durability of Wood-Thermoplastic Composite Materials in Simulated Marine Environments" –Proceedings of the *Society of Experimental Mechanics (SEM) Conference* , June 1999, Cincinnati, OH.

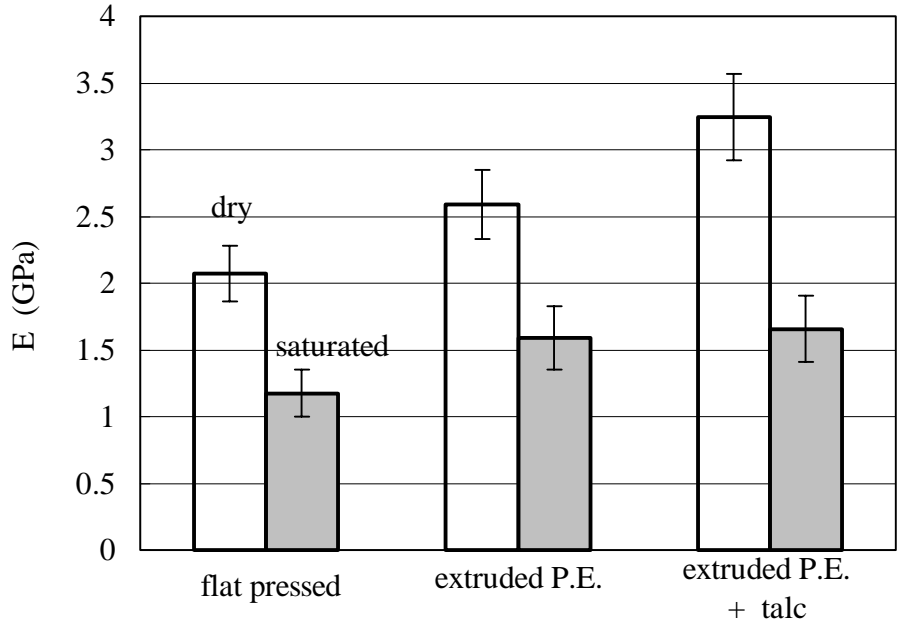


Fig. 4.1(a): Comparison of static stiffness (average value and scatter band shown)

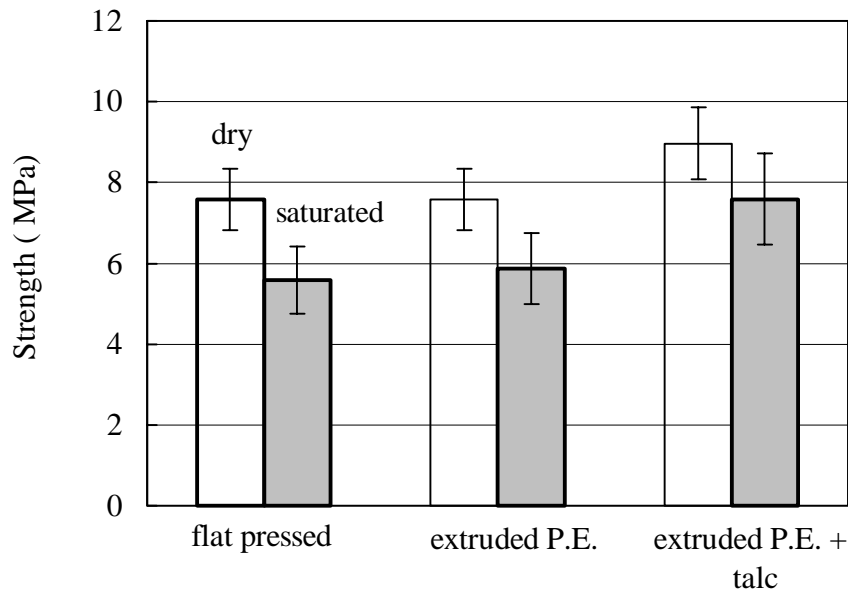


Fig. 4.1(b): Comparison of static strength

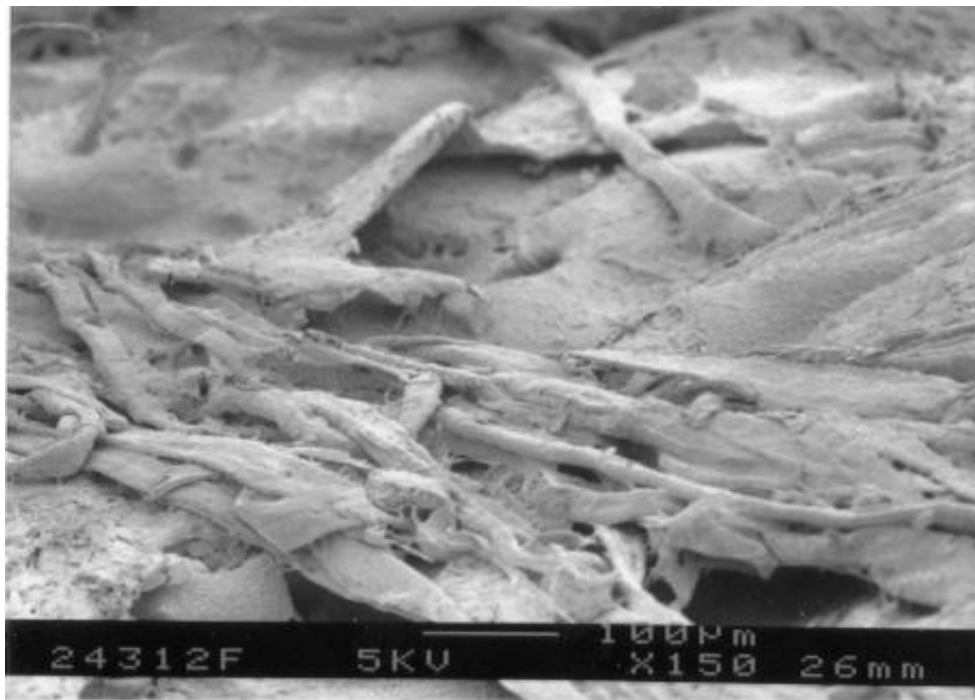
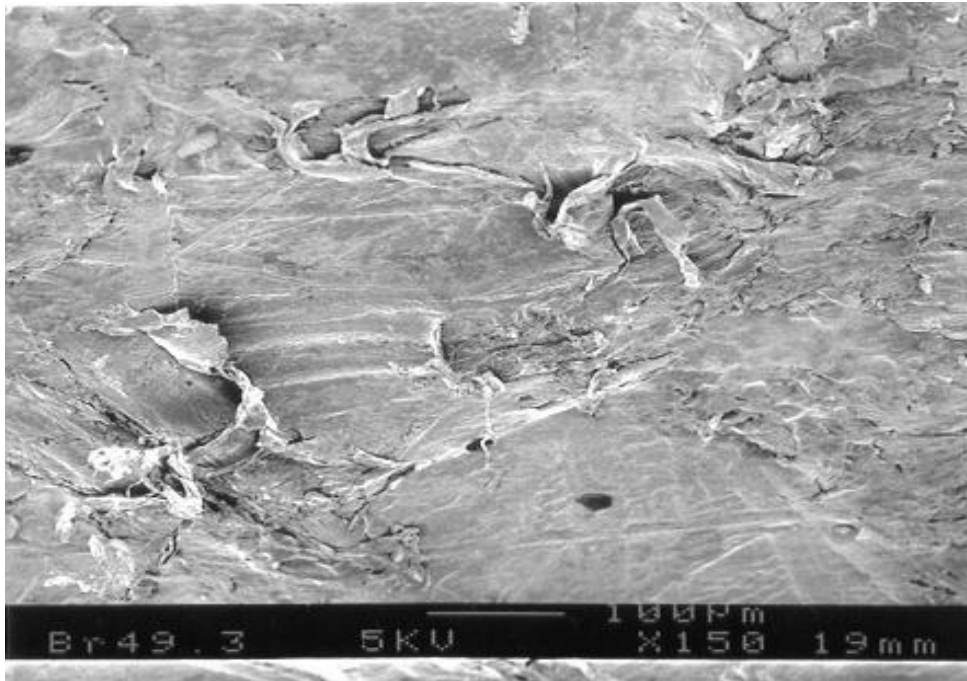


Fig. 4.2 : Microscopic (150 magnification) surface images of flat pressed coupons, dry (top) and saturated (bottom) coupons.

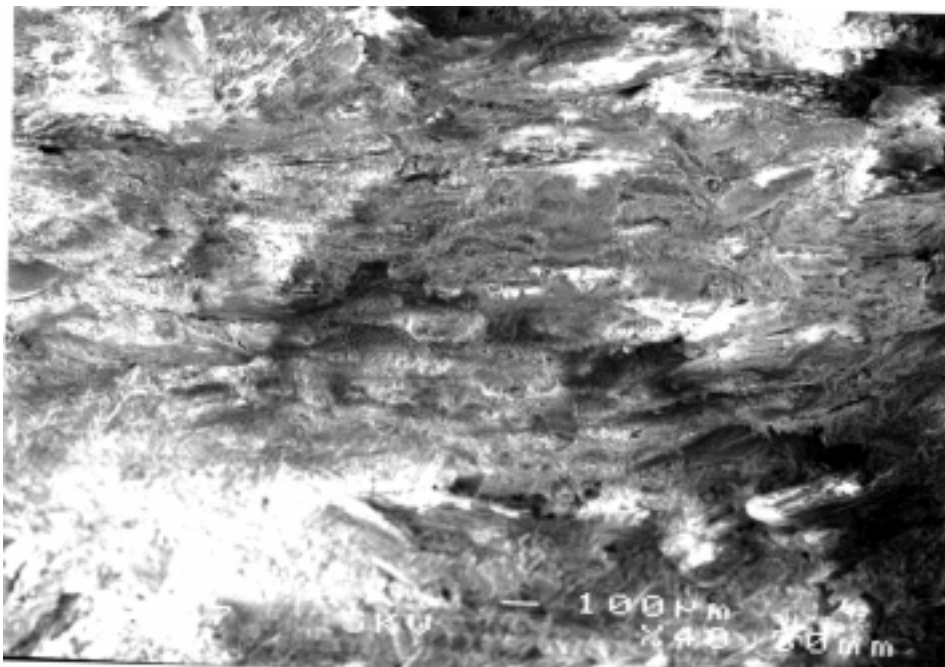
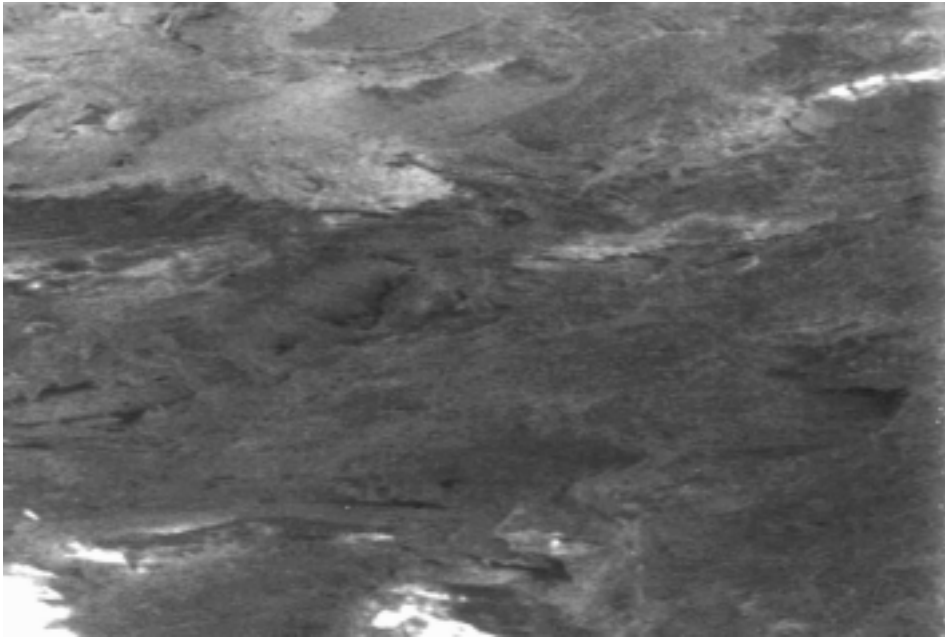


Fig. 4.3: Microscopic images (40 magnification) of fracture surface, dry (top) and saturated (bottom) coupons.



Fig. 4.4: Microscopic images showing particle matrix interface on the fracture surface of a dry (top) and saturated in seawater (bottom) extruded P.E. coupon.

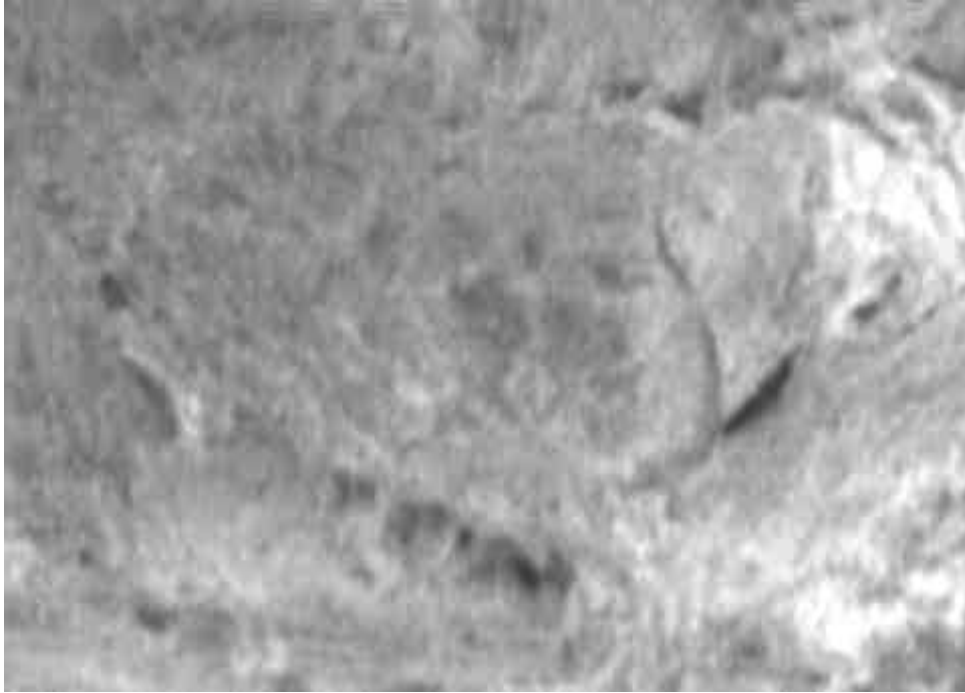


Fig. 4.5: Microscopic images showing particle matrix interface on the fracture surface of a dry (top) and saturated in seawater (bottom) flat pressed coupon.

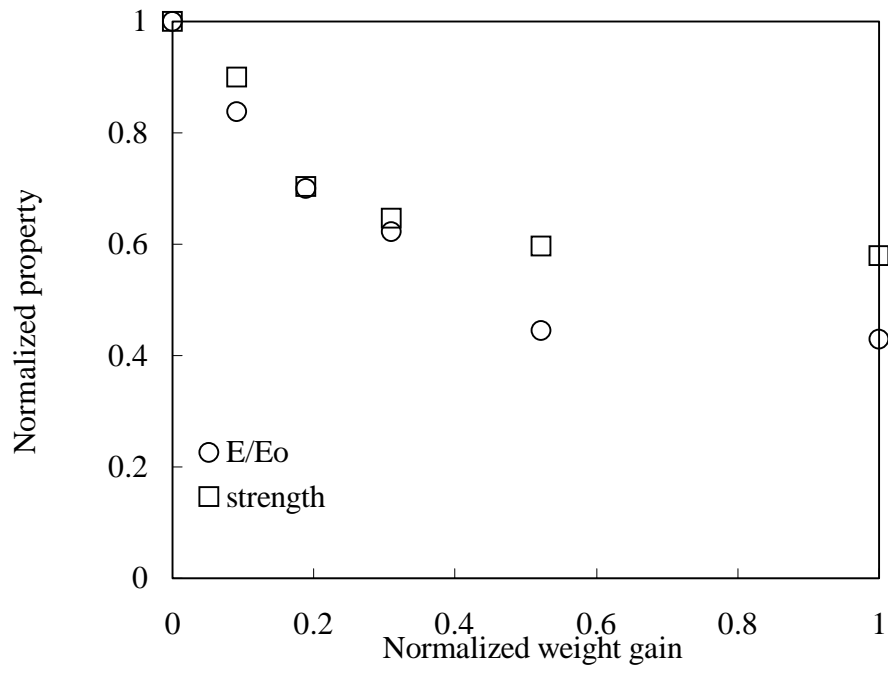


Fig. 4.6: Stiffness and strength reduction during sorption for flat pressed coupons

CHAPTER FIVE

FATIGUE RESPONSE OF THE FLAT PRESSED MATERIAL

5.1 Introduction

Fatigue tests were conducted to characterize the fatigue response of the flat pressed material and investigate the effects of moisture on fatigue life. Under immersed conditions moisture transport may occur by diffusion and capillary action through load induced cracks developing in the coupon (Smith and Weitsman, 1996), (Bradley and Chiou, 1992). The water trapped inside these cracks can act synergistically with the applied load, to alter the stress state in the coupon, accelerate fatigue damage and lower the fatigue life. In the presence of hygrothermal damage, the reduced static strength and stiffness associated with diffusion may further lower the fatigue life. It is unclear however, whether the interaction of damage and moisture play an important role for the material under consideration.

In the following, fatigue data for the flat pressed material is presented in the form of S-N curves. The material damage (degradation in stiffness and strength) accompanying cyclic loading manifests itself in the form of a reduction in stiffness along the loading direction. This is monitored by a continuous in-situ measurement of the coupon stiffness during the fatigue life, which enables the measurement of a damage rate. This damage rate is shown to depend on the maximum stress in the fatigue cycle. The combined effect of fluid exposure and cyclic loading is investigated by subjecting saturated and dry coupons to cyclic loading when immersed in seawater. It is shown that during immersed fatigue, the combined effect of fluid transport (capillary action and diffusion) and

sorption induced damage, reduce the fatigue life of the material and accelerate the damage progression.

5.2 Test setup and materials

The fatigue tests were conducted on a 4 post 44 kN (20 kip) servohydraulic load frame in load control, according to guidelines prescribed in ASTM D3479. Coupon geometry and cutting operations were similar to that used in the moisture sorption studies (3.3). The test was controlled using an MTS 407 controller. During the fatigue test, the peak load, valley load, peak strain and valley strain in each fatigue cycle was recorded using a computer data acquisition system. Strain measurements were made using an extensometer clipped to the surface of the coupon and a Vishay 2110A signal conditioner. Coupon stiffness was calculated from the slope of the load-strain data during loading in each fatigue cycle. To monitor damage progression, the coupon stiffness was measured at regular intervals from in-situ measurements of coupon strain and load. To investigate the combined effects of saturation and immersion on fatigue response, the fatigue tests were done under the following three test conditions:

1. Dry coupons fatigued in air,
2. Saturated coupons, fatigued immersed in seawater,
3. Dry coupons, fatigued immersed in seawater.

For each of these three test conditions, tests were performed at four load levels. All tests were done at a cycle frequency of 5 Hz. To perform the immersed fatigue tests, the coupons were enclosed in a compliant plastic bag filled with seawater. The seawater was replenished from time to time to make up for water loss due to possible leakage in the bag.

The fatigue tests were done with the maximum stress (σ_{\max}) in the cycle as 95%, 85%, 70% and 60% of ultimate tensile strength (S_{ut}) of the material. A cycle frequency of 5 Hz and R ($\sigma_{\min}/\sigma_{\max}$) ratio of 0.1 was used for all tests. Due to the inherent scatter associated with dynamic tests, seven replicate tests were performed at each load.

5.3 Results and discussion

5.3.1 Influence of saturation and immersion on fatigue behavior

S-N data for the flat pressed material tested under the three conditions described above is shown in **Fig. 5.1**. As seen in **Fig. 5.1**, dry coupons tested immersed have a lower fatigue life than those tested in air, and the saturated coupons tested immersed have the lowest fatigue life. During immersed fatigue, the coupons experience loss of stiffness and strength from moisture sorption induced damage. Further, there can also be transport of fluid into the coupon by capillary action through the surface microcracks produced by fatigue loading. Such trapped fluid inside the cracks is known to accelerate their growth due to the synergistic effect of capillary action, diffusion and cyclic loading.

In this case, the reduced fatigue life of saturated coupons tested immersed may be due to sorption. To isolate the influence of sorption on fatigue life of the saturated coupons tested immersed, the data of **Fig. 5.1** is normalized with their static strength in **Fig. 5.2**. Accordingly, the effect of sorption appears significant, and probably larger than the capillary effects that may be present. From the short cycle tests ($N < 10^5$) of the dry coupons tested immersed, it appears that the capillary action may not have as much of an effect on fatigue life as sorption. The reduced fatigue life of the dry coupons tested immersed is only apparent

for the longer duration tests ($N > 10^5$), and appears to be due to diffusion occurring during the test (**Fig. 4.3**).

5.3.2 Model for fatigue life

Fatigue life may be empirically represented using a power law (Talreja, 1988) as

$$N_f \cdot S^m = C \quad (5.1a)$$

Taking the logarithm of both sides, Eq. (5.1a) becomes a straight line commonly observed in fatigue studies.

$$\text{Log}(S) = \left(\frac{-1}{m}\right) \cdot \text{Log}(N_f) + \frac{1}{m} \cdot \text{Log}(C) \quad (5.1b)$$

To scale out the coupon to coupon variability, the maximum stress in the cycle (σ_{\max}) is normalized with the coupon stiffness in the first load cycle (E_0). Hence, the parameter S is the maximum first-cycle strain, N_f is the number of cycles to failure (fatigue life), C and m are constants that depend upon the material and test condition (i.e. environment). Correlation between the model and data for the dry coupons tested in air is shown in **Fig. 5.3**.

5.3.3 Damage accompanying fatigue loading

Damage during fatigue loading was measured by continuously monitoring the coupon stiffness as described earlier (5.2). A plot of the coupon's stiffness during its fatigue life shown in **Fig. 5.4**, and can be divided into three distinct regions. Region 1 shows a rapid

decrease in coupon stiffness over the first few cycles, the extent of damage in this region correlated with the amount of damage observed in a quasi-static loading-unloading test to the same load. This, then stabilizes into a linear region 2. Finally just prior to failure, a rapid decrease in stiffness is again observed, which is region 3 that may be associated with localization of damage in the failure zone.

By convention, the slope of the linear region 2 (dE/dt or dE/dN) was used as a measure of the damage rate. The damage rate was observed to depend on the maximum stress in the fatigue cycle and the test environment (dry or immersed), this is illustrated in **Fig. 5.5**. In **Fig. 5.5** the values of dE/dt were normalized with the coupon stiffness in the first loading cycle (E_0). This normalized form of the damage rate $(dE/dt)_N$ accounts for the macro-level coupon to coupon variability and helps minimize the scatter in the data. Saturated coupons tested immersed had higher damage rates, particularly for the short duration, high stress tests.

5.4 Conclusions

Fatigue studies for the flat pressed material indicate that moisture can have a significant effect of fatigue life and damage growth. Damage from moisture transport by capillary action may still be present, however sorption induced damage seemed to be the more dominant cause for the reduction in fatigue life of the saturated coupons tested in immersed environments.

The progression of damage during the fatigue life can be quantified by measuring the modulus reduction along the loading direction. The fatigue life data can be modeled by a power law expression based on maximum first cycle strain. Good correlation between this model and the data for the flat pressed material was obtained.

5.5 References

- 1] Smith, L.V., and Weitsman, Y.J., "The Immersed Fatigue Response of Polymer Composites," *International Journal of Fracture*, 82: 31-42, 1996.
- 2] Bradley, W. L., and Chiou, P. -L. B., "The Effect of seawater Exposure on the Fatigue Behavior of a Polymeric Composite," *Materials Engineering, ASME, OMAE*, 3: 175-179, 1992.
- 3] American Society for Testing of materials, "Standard Test Method for Tension-Tension Fatigue of Oriented Fiber, Resin Matrix Composites," *ASTM D 3479-76*, 145-147, 1990.
- 4] Talreja, R., "Fatigue of Composite Materials," *Technomic Publishing Co. Inc.*, 1987.
- 5] Corum, J. M., Simpson, Jr. W. A., Sun, C. T., Talreja, R., Weitsman, Y. J., "Durability of Polymer Matrix Composites for Automotive Structural Applications: A State-of-the-Art Review," *Oak Ridge National Laboratory*, Report No. ORNL-6869.
- 6] Frederic, P., Leif, A. C., and John, W., Gillespie, Jr., "Marine Environmental Effects on Polymer Matrix Composites," *Composite Materials: Fatigue and Fracture, ASTM STP 1230*, Martin, R. H., Ed., American Society for Testing and Materials, Philadelphia, 5: 283-303, 1993.

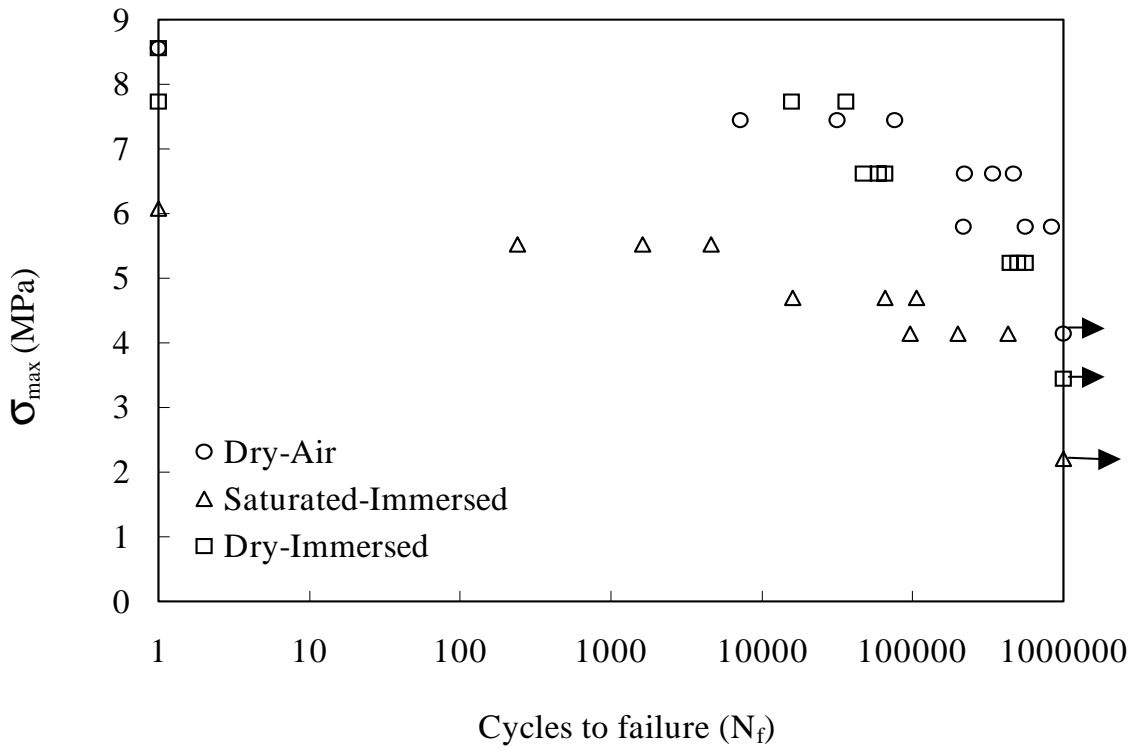


Fig. 5.1: Fatigue data for flat pressed material (arrows indicate tests stopped after 10^6 cycles)

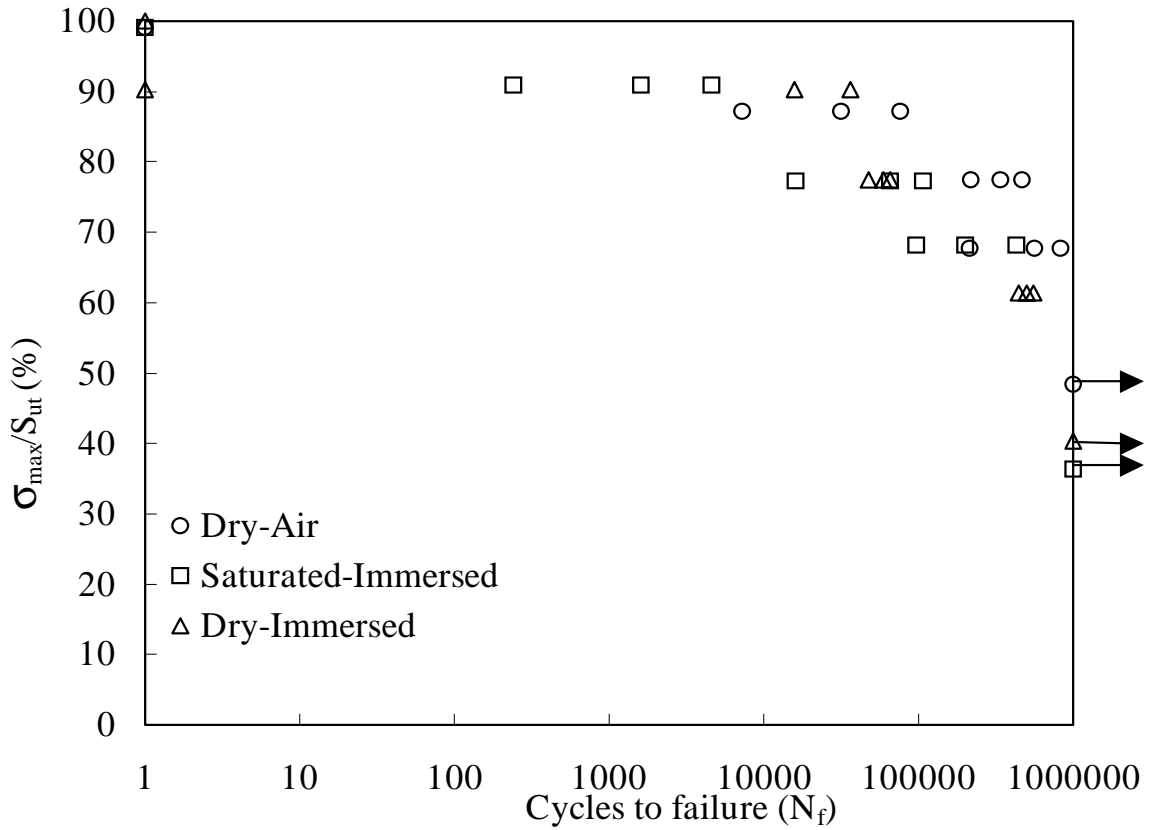


Fig. 5.2: Fatigue data for flat pressed material based on percent of ultimate stress

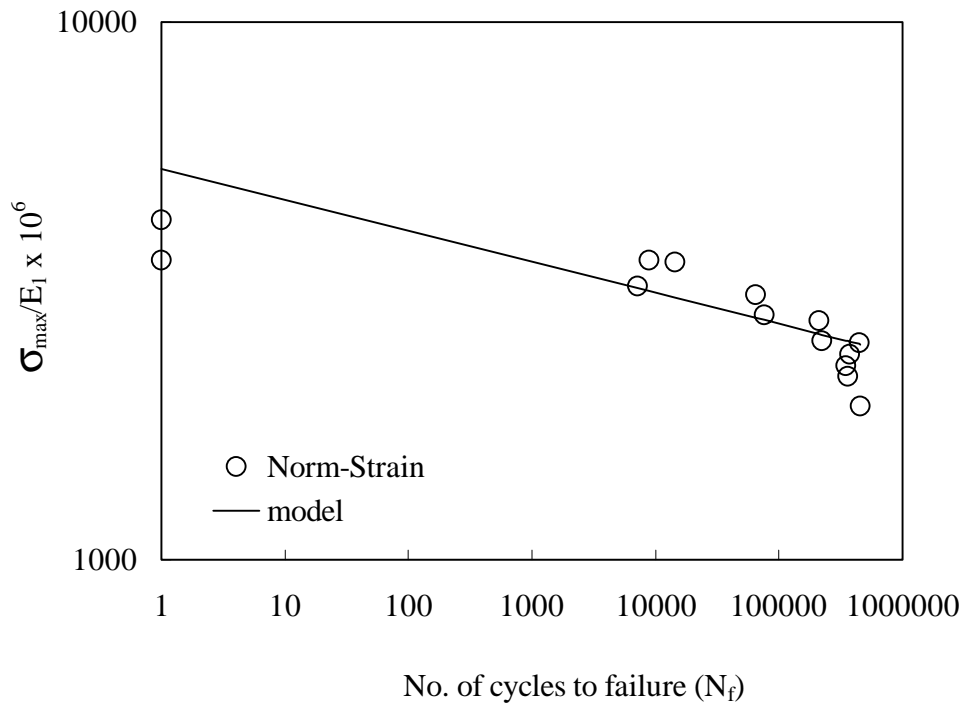


Fig. 5.3: Correlation between fatigue life model Eq. (5.1) and data for the flat pressed material

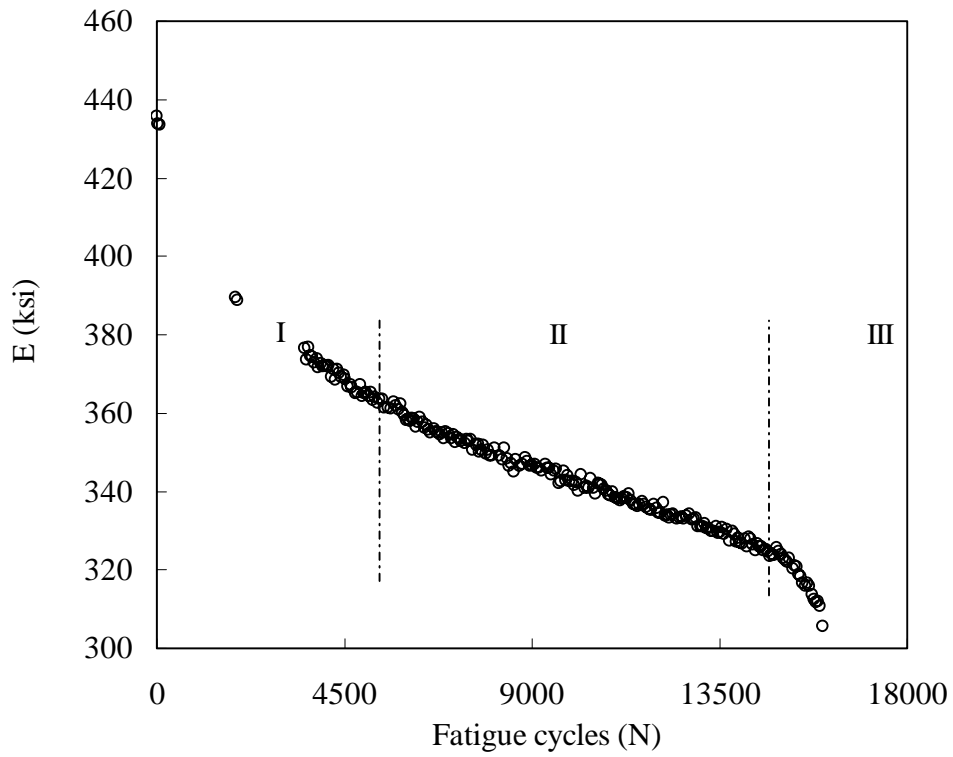


Fig. 5.4: Stiffness reduction during fatigue loading (90% Sut)

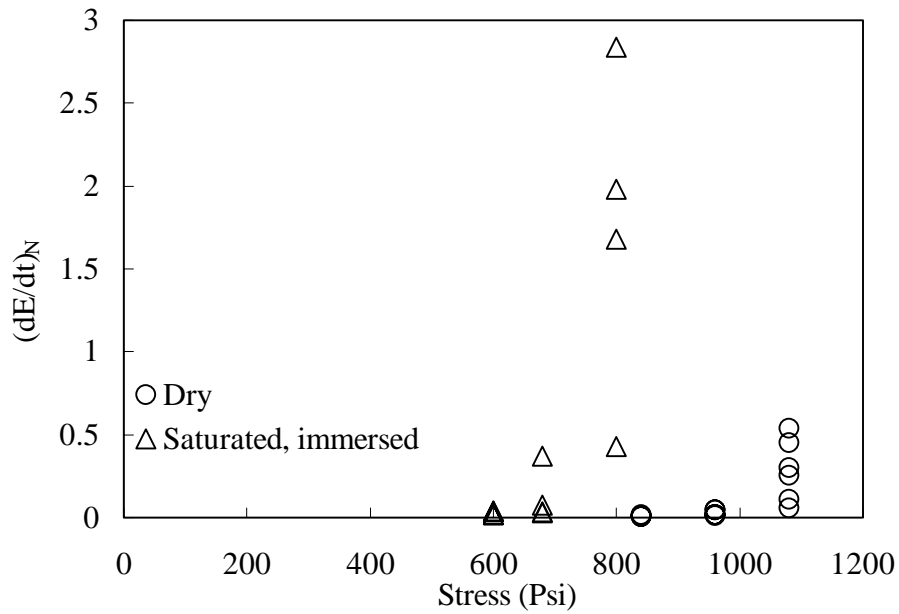


Fig. 5.5: Comparison of normalized damage rates for dry and saturated-immersed fatigue tests

CHAPTER SIX

VISCOELASTIC RESPONSE OF THE FLAT PRESSED MATERIAL

6.1 Introduction

This chapter considers the creep response of the flat pressed material. The characterization study is based on creep and recovery tests of various creep stress amplitudes and durations. Damage and permanent deformation were observed in the material when the creep stress amplitude exceeded a threshold value. The damage and plasticity were found to have an instantaneous stress dependent component and a time dependent component. The permanent deformation was more efficiently accommodated by considering the coupon total strain, however. The purpose of this study was to develop a predictive model incorporating the observed time dependence, damage effects and plastic deformation. A non-linear viscoelastic model is presented that incorporates the effects of damage and permanent deformation. Damage was modeled by considering an effective stress. The model is shown to compare favorably with the experimental creep/recovery data as well as two step load history verification tests.

The results of quasi-static tension tests are presented that determine material properties and assess the extent of variability in the material. These are followed by the creep characterization tests to assess time dependence and damage. A viscoelastic model, incorporating the effects of instantaneous damage, time dependent damage and permanent deformation, is developed. Correlations between the prediction from the model and experimental data at various creep stresses and durations are then presented.

Finally, the capability of the model is assessed by correlating its predictions with data from two step load histories.

6.2 Quasi-static tension tests

Quasi-static tension tests were performed to determine the static strength and stiffness, identify the linear range of the stress-strain response and assess the variability in the material. Coupon geometry and cutting operations for these tests were similar to that used in the moisture sorption studies (3.3).

A representative stress-strain curve is shown in **Fig. 6.1** for a coupon loaded to 85% of its ultimate tensile strength (S_{ut}). As may be observed from the figure, the stress-strain response is linear up to approximately 2.76 MPa (400 psi) (33% S_{ut}). Stiffness was therefore measured as the chord modulus between 0.69 MPa (100 psi) and 2.76 MPa (400 psi). The Young's moduli (measured from 24 coupons taken from 12 different flat pressed panels) ranged between 1900 MPa (275 ksi) to 2270 MPa (330 ksi) with a mean value of 2100 MPa (300 ksi) and standard deviation of 123 MPa (17.8 ksi). The corresponding ultimate tensile strength (S_{ut}) values ranged from 6.6 MPa (0.96 ksi) to 9.6 MPa (1.38 ksi) with a mean value of 8.2 MPa (1.2 ksi) and standard deviation of 1.07 MPa (0.15 ksi).

6.3 Creep characterization tests

6.3.1 Test set-up

The creep tests consisted of the application of a step stresses σ_0 and their removal after various durations t_0 as shown in **Table 6.1**. Subsequent to load removal the coupons

were allowed to relax for a duration of $3t_0$ during which the recovery data was collected. All the tests were performed on a 4 post 44 KN (20 kip) M.T.S servo-hydraulic load frame. Strains were measured using an extensometer clipped on to the surface of the coupon and a Vishay 2110A signal conditioner. Labview software was used for data acquisition. Coupon geometry and cutting operations for the creep tests similar to that used in the moisture sorption studies (3.3).

Loading and unloading in step fashion cannot be realized in practice. A constant loading rate of 44.5 N/s (10 lb./s) was used here, requiring 5-10 seconds to attain prescribed stress levels. This finite loading time allowed measurement of the loading and unloading compliances. Creep tests were done at creep stresses in the linear and non-linear ranges as indicated in **Table 6.1**.

Table 6.1: Creep test matrix. (Column entries indicate number of replicate tests)

Creep Stress (MPa), (%Sut)	0 min	15 min	30 min	60 min	120 min	240 min
1.72 (20%)	4	5	5	4	4	3
2.76 (33%)	4	5	5	4	4	3
4.69 (55%)	4	5	5	4	4	3
5.79 (70%)	4	5	5	4	4	3

6.3.2 Creep response in the linear range

From the static tests, the linear range was found to be $\sigma_0 < 2.76$ MPa (400 psi) and $\varepsilon(t) < 1400 \mu\varepsilon$. Below this threshold the creep strain $\varepsilon(t)$ is proportional to the creep stress σ_0 , and damage effects were not observed. The time dependent compliance was modeled using a power law of the form (Jerina et al., 1982)

$$D(t) = D_0 + D_1 \cdot t^n \quad (6.1)$$

The time dependent strain may be found by evaluating the convolution integral (Flugge, 1967 and Fung, 1965)

$$\varepsilon(t) = \int_{-\infty}^t D(t - \tau) \cdot \frac{d}{d\tau} \sigma(\tau) d\tau \quad (6.2)$$

Given a step input in stress, $\sigma(t) = \sigma_0 H(t)$, where $H(t)$ is the heavyside step function, the resulting time dependent strain is readily obtained as

$$\begin{aligned} \varepsilon(t) &= (D_0 + D_1 \cdot t^n) \cdot \sigma_0 & 0 < t < t_0 \\ \varepsilon(t) &= D_1 \cdot [t^n - (t - t_0)^n] \cdot \sigma_0 & t > t_0 \end{aligned} \quad (6.3)$$

In Eq. (6.3), D_0 , D_1 and n are material parameters, σ_0 is the creep stress and t_0 is the creep duration. If the loading rate is sufficiently rapid that time dependent effects during loading are negligible, D_0 can be determined from the slope of the stress-strain data during loading. Since the expression for recovery does not contain D_0 ; D_1 and n were determined from recovery data. Correlation between Eq. (6.3) and a representative

coupon in the linear range for creep and recovery is presented in **Fig. 6.2**. While the model does not capture all of the features of the data in **Fig. 6.2**, it provides a reasonable fit, given the coupon to coupon variability and signal noise associated with measuring relatively small recovery strains.

More variability was observed for the instantaneous compliance, D_0 , than for D_1 and n where $318 < D_0 < 405 \mu\epsilon/\text{MPa}$ ($2.2 < D_0 < 2.8 \mu\epsilon/\text{psi}$), $D_1=30 \mu\epsilon/\text{Mpa-min.}$ ($0.208 \mu\epsilon/\text{psi-min.}$) and $n=0.4$. The variation in D_0 can be attributed to the lack of repeatability in the flat pressing process. It is essential, therefore, to have normalization schemes to scale out this variability.

6.3.3 Non-linear response

The dependence of damage on creep stress and duration were studied by conducting tests at various stresses and durations above σ_d . The existence of damage was established by an increased compliance, measured while the creep load was removed. Damage was expressed as the ratio of the unloading and loading compliances (D_u/ D_L). This ratio reduces the coupon to coupon variability, normalizing instantaneous compliance variation and is plotted vs. creep stress and duration in **Fig. 6.3**. The dependence of damage on creep stress and duration suggests that it has an instantaneous, stress dependent, component and a time dependent component. The total creep strain is hence affected by two time scales, one due to creep and the other due to growing damage. In the presence of time dependent damage a transition from secondary to tertiary creep was observed when the stress level is sufficiently high ($\sigma_0=85\% S_{ut}$).

Permanent deformation after recovery was observed for coupons loaded into the non-linear range. The permanent strain increased with creep stress and duration as shown in **Fig. 6.4**. The large scatter in the permanent strain may be attributed to variations in initial compliance. When the permanent strain ϵ_p was plotted against the maximum creep strain (as shown in **Fig. 6.5**) a linear dependence was observed as

$$\epsilon_p = K_p \cdot (\epsilon_{\max} - \epsilon_d) \cdot H(\epsilon_{\max} - \epsilon_d) \quad (6.4)$$

Recall that ϵ_{\max} depends on σ_0 and t_0 , hence Eq. (6.4) shows an implicit dependence of ϵ_p on σ_0 and t_0 .

To incorporate the effects of damage into the creep model, the concept of effective stress was used (Lemaitre and Chaboche, 1990). This effective stress is the applied stress acting over the effective area in a damaged material. The deformation behavior of the damaged material is represented by the constitutive laws of the undamaged material in which the applied stress is replaced by the effective stress σ_e , which is given by

$$\sigma_e(t, \sigma_0) = K_T \cdot \sigma_0 \quad (6.5)$$

In Eq. (6.5), σ_0 is the applied creep stress and K_T is a damage function. Given the observed instantaneous and time dependent damage, K_T should increase with stress and creep duration. Since damage showed a linear dependence on creep stress and duration (**Fig. 6.3**), the following function was chosen for K_T

$$K_T(\sigma_0, t) = A(\sigma_0 - \sigma_d) + B(\sigma_0 - \sigma_d) \cdot t \quad (6.6a)$$

Where

$$\begin{aligned} A(\sigma_0 - \sigma_d) &= 1 + K_{dA} \cdot (\sigma_0 - \sigma_d) \cdot H(\sigma_0 - \sigma_d) \\ B(\sigma_0 - \sigma_d) &= K_{dB} \cdot (\sigma_0 - \sigma_d) \cdot H(\sigma_0 - \sigma_d) \end{aligned} \quad (6.6b)$$

Values for A and B were empirically determined for coupons exposed to various magnitudes and durations of creep stress to provide the best fit with the strain data, as shown in **Fig. 6.6**. The constants K_{dA} and K_{dB} represent the slopes of the straight lines through the average values of A and B at each stress. For the material at hand $K_{dA}=0.188 \text{ MPa}^{-1}$ ($1.3 \times 10^{-3} \text{ psi}^{-1}$), $K_{dB}=2.89 \times 10^{-3} \text{ MPa}^{-1}\text{min.}^{-1}$ ($2 \times 10^{-5} \text{ psi}^{-1}\text{min.}^{-1}$). (In the linear range, where damage is absent, we would have $A=1$ and $B=0$.)

Combining Eq. (6.5) and (6.6) the effective stress for creep and recovery, respectively become

$$\begin{aligned} \sigma(\tau) &= \sigma_0 \cdot (A + B \cdot \tau) \cdot H(\tau) & 0 < \tau < t_0 \\ \sigma(\tau) &= \sigma_0 \cdot (A + B \cdot \tau) \cdot H(\tau) - \sigma_0 \cdot (A + B \cdot \tau) \cdot H(\tau - t_0) & \tau > t_0 \end{aligned} \quad (6.7)$$

The non-linear time dependent strain may be found by evaluating the convolution integral with the effective stress from Eq. (6.7). Expressions for creep and recovery strains, respectively, yield

$$\varepsilon(t) = \sigma_0 \cdot A \cdot \left(D_0 + D_1 \cdot t^n \right) + \sigma_0 \cdot B \cdot \left(D_0 \cdot t + \frac{D_1}{n+1} \cdot t^{n+1} \right) \quad 0 < t < t_0$$

Eq. (6.8) does not account for the observed permanent deformation however. Following established procedures (Smith and Weitsman, 1996) the total creep strain can be resolved into viscoelastic and plastic components as

$$\begin{aligned}\varepsilon(t) &= \sigma_0 \cdot A \cdot (D_0 + D_1 \cdot t^n) + \sigma_0 \cdot B \cdot \left(D_0 \cdot t + \frac{D_1}{n+1} \cdot t^{n+1} \right) & 0 < t < t_0 \\ \varepsilon(t) &= \sigma_0 \cdot A \cdot D_1 \cdot \left[t^n - (t - t_0)^n \right] + \sigma_0 \cdot B \cdot \frac{D_1}{n+1} \left[t^{n+1} - (t - t_0)^{n+1} \right] - \sigma_0 \cdot B \cdot D_1 \cdot t_0 \cdot (t - t_0)^n & t > t_0\end{aligned}\quad (6.8)$$

Eq. (6.8) does not account for the observed permanent deformation however. Following established procedures (Smith and Weitsman, 1996) the total creep strain can be resolved into viscoelastic and plastic components as

$$\varepsilon(t) = \varepsilon_p(t) + \varepsilon_v(t) \quad (6.9)$$

The previously determined relation between the plastic strain and the total creep strain (Eq. 6.3) can be used to determine a recovery strain that accounts for plastic deformation. Evaluating Eq. (6.9) for creep and recovery yields

$$\begin{aligned}\varepsilon_T(t) &= \varepsilon_v(t) + \varepsilon_p(t) & 0 < t < t_0 \\ \varepsilon_r(t) &= \varepsilon_v(t) - \varepsilon_v(t - t_0) + \varepsilon_p(t_0) & t > t_0\end{aligned}\quad (6.10)$$

$$\begin{aligned}\varepsilon_v(t) &= \varepsilon_T(t) & \varepsilon < \varepsilon_d \\ \varepsilon_v(t) &= \varepsilon_T(t) - \varepsilon_p(t) & \varepsilon > \varepsilon_d\end{aligned}\quad (6.11)$$

Eq. (6.11) may be evaluated with Eq. (6.4) for the case of $\varepsilon > \varepsilon_d$ to yield

$$\begin{aligned}\varepsilon_v(t) &= \varepsilon_T(t) - K_p \cdot [\varepsilon_T(t) - \varepsilon_d] \\ \varepsilon_v(t) &= \varepsilon_T(t) \cdot (1 - K_p) + K_p \cdot \varepsilon_d\end{aligned}\quad (6.12)$$

The viscoelastic component of the strain is then found by combining Eq. (6.8) and Eq. (6.12) as

$$\varepsilon_v(\sigma_0, t) = (1 - K_p) \cdot \left[A \cdot \sigma_0 \cdot (D_0 + D_1 \cdot t^n) + B \cdot \sigma_0 \cdot \left(D_0 \cdot t + \frac{D_1}{n+1} \cdot t^{n+1} \right) \right] + K_p \cdot \varepsilon_d \quad (6.13)$$

The plastic component of the strain is found by combining Eq. (6.4) and Eq. (6.8) as

$$\varepsilon_p(\sigma_0, t_0) = K_p \cdot \left[A \cdot \sigma_0 \cdot [D_0 + D_1 \cdot (t_0)^n] + B \cdot \sigma_0 \cdot \left[D_0 \cdot t_0 + \frac{D_1}{n+1} \cdot (t_0)^{n+1} \right] - \varepsilon_d \right] \quad (6.14)$$

Correlations between Eq. (6.10) and representative coupons in the non-linear range at different creep stresses and durations are shown in Figs. 6.7 and 6.8.

6.4 Model Verification Tests

Two step creep and recovery tests

Tests that differed in kind from the characterization work were performed to assess the predictive capability of the model. The coupons were subjected to two step creep and recovery cycles in the non-linear range. In the first cycle, the coupon was subjected to a creep stress σ_1 for a duration t_{01} . (After which recovery for an extended period t_r ($t_r > 50 t_{01}$) was allowed.) Subsequently, the coupon was subjected to a creep stress σ_2 for a duration t_{02} . Cases with $\sigma_1 < \sigma_2$ and $\sigma_1 > \sigma_2$ were considered. Since time dependent damage was encountered in the material at hand a third type of test in which $\sigma_1 = \sigma_2$ and $t_{02} > t_{01}$ was performed. Strain and time were reset to zero after the first step before recording data for the second step. The creep and recovery strains for the second step for increasing stress are given by

$$\begin{aligned}\varepsilon(t) &= \varepsilon_v(\sigma_2, t) + \varepsilon_p(\sigma_2, t) - \varepsilon_p(\sigma_1, t_{01}) & 0 < t < t_0 \\ \varepsilon(t) &= \varepsilon_v(\sigma_2, t) - \varepsilon_v(\sigma_2, t - t_{02}) + \varepsilon_p(\sigma_2, t_{02}) - \varepsilon_p(\sigma_1, t_{01}) & t > t_0\end{aligned}\quad (6.15)$$

For decreasing stress, the creep and recovery strains for the second step are found from

$$\begin{aligned}\varepsilon(t) &= \left[\varepsilon_v(\sigma_1, t) + \varepsilon_p(\sigma_1, t) - \varepsilon_p(\sigma_1, t_{01}) \right] \cdot \frac{\sigma_2}{\sigma_1} & 0 < t < t_0 \\ \varepsilon(t) &= \left[\varepsilon_v(\sigma_1, t) - \varepsilon_v(\sigma_1, t - t_{02}) - \varepsilon_p(\sigma_1, t_{01}) \right] \cdot \frac{\sigma_2}{\sigma_1} & t > t_0\end{aligned}\quad (6.16)$$

Correlations between Eq. (6.15) and Eq. (6.16) and representative coupons are shown in **Figs. 6.9, 6.10 and 6.11.**

6.5 Conclusions

The material at hand exhibited time dependent behavior at all stress levels, which may be attributed to the significant volume fraction of the thermoplastic matrix. The creep model, based on a power law, adequately represents the response of the material in the linear and non-linear ranges (if damage effects are included). The predictive capability of the model was limited by the inherent variability associated with the flat-pressing process and the signal noise associated with measuring relatively small recovery strains.

The effect of damage on the creep response was modeled by considering an effective stress. Permanent strains were accounted for by resolving the total creep strain into viscoelastic and viscoplastic components and utilizing a relationship between viscoplastic strain and total strain.

The applicability of this model to the creep response of similar wood-thermoplastic composite materials made by incorporating other additives and by alternate processing methods is currently under investigation.

6.6 References

- 6.1] Smith, L.V., and Weitsman, Y.J., “Inelastic Behavior of Randomly Reinforced Polymeric Composites under Cyclic Loading,” *Mechanics of Time-Dependent Materials*, 1: 293-305, 1998.
- 6.2] Smith, L.V., and Weitsman, Y.J., “The Visco-Damage Mechanical Response of Swirl-Mat Composites,” *International Journal of Fracture*, (to appear).
- 6.3] Corum, J. M., Simpson, Jr. W. A., Sun, C. T., Talreja, R., Weitsman, Y. J., “Durability of Polymer Matrix Composites for Automotive Structural Applications: A State-of-the-Art Review,” *Oak Ridge National Laboratory*, Report No. ORNL-6869.
- 6.4] Upadhyay, P.C., and Mishra, A., “Parametric Modeling of Moisture Assisted Creep in Polymeric Composites,” *Journal of Reinforced Plastics and Composites*, 13: 1057-1070, 1994.
- 6.5] Lemaitre, J., and Chaboche, J. –L., “Mechanics of Solid Materials,” *Cambridge University Press*, 57, 1990.
- 6.6] Chia, L. H. L., Teoh, S. H., and Boey, F. Y. C., “Creep Characteristics of a Tropical Wood-Polymer Composite,” *Radiation Physics and Chemistry*, 29-1: 25-30, 1987.
- 6.7] Jerina, K. L., Schapery, R. A., Tung, R. W. and Sanders, B. A., “Viscoelastic Characterization of a Random Fiber Composite Material using Micromechanics”, *Short Fiber Reinforced Composite Materials*, B. A. Sanders (ed.), ASTM STP 772, ASTM, Philadelphia, 225-250, 1982.
- 6.8] Flugge, W., “Viscoelasticity,” *Blaisdell Publishing Company*, 1967.
- 6.9] Fung, Y. C., “Foundations of Solid Mechanics,” *Prentice Hall, Inc.*, 1965.

6.10] Rangaraj, S. V., and Smith, L. V., “Non-Linear Viscoelastic Response of a Wood-Thermoplastic Composite Material” – in review, *Mechanics of Time Dependent Materials*.

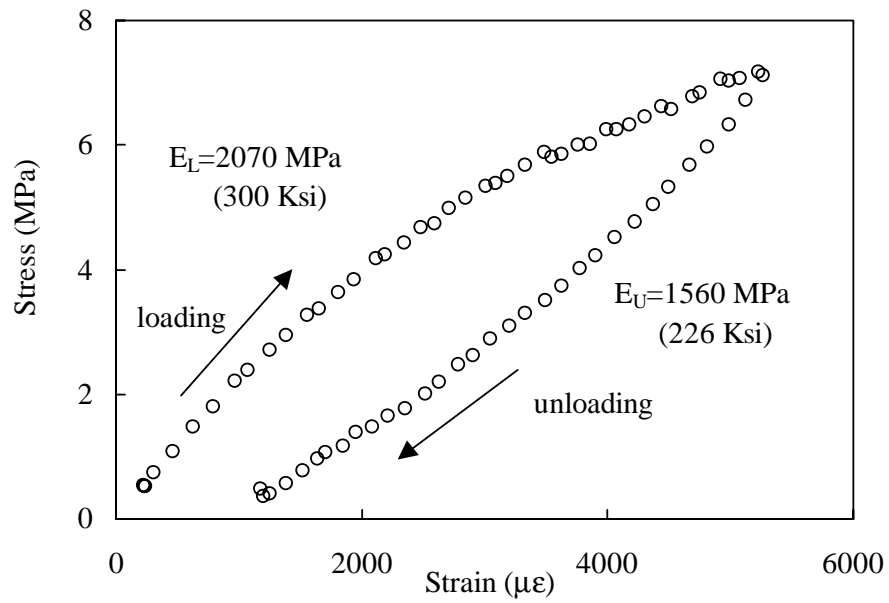


Fig. 6.1: Quasi-static tension test in the non-linear range, (E_L and E_U are loading and unloading moduli respectively)

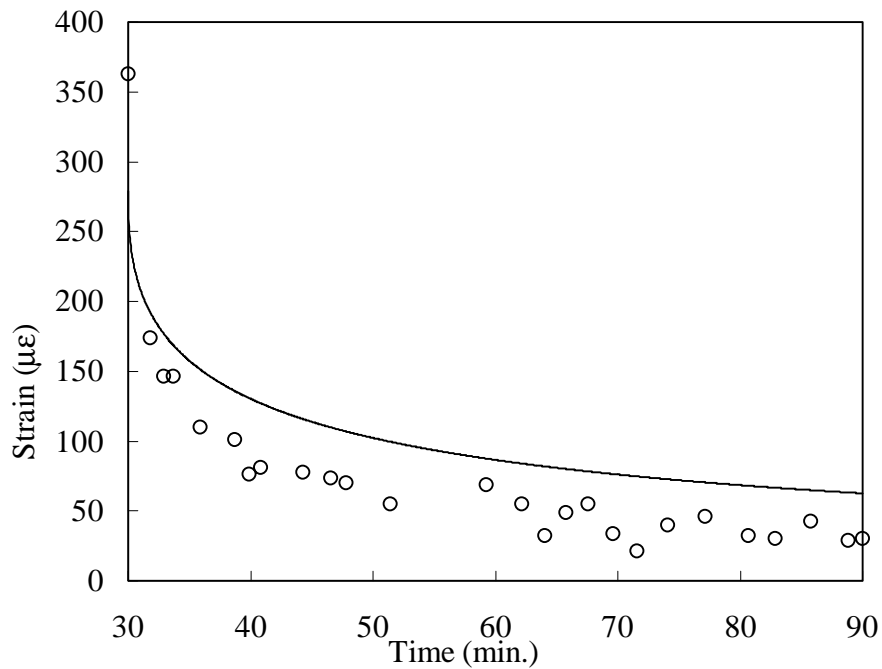
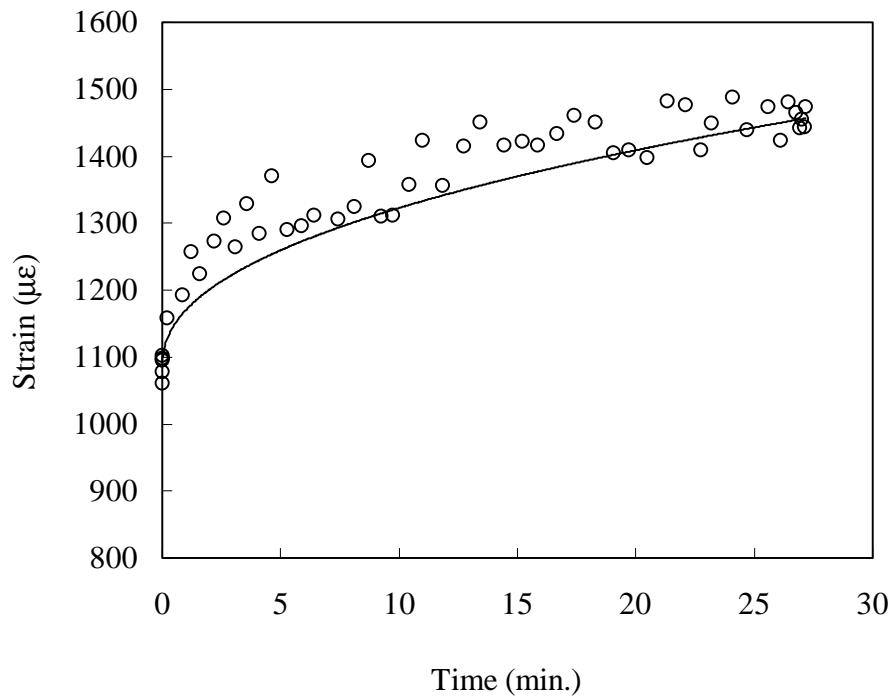


Fig. 6.2 : Comparison between Eq.(6.3) and a representative coupon in the linear range for creep (top) and recovery (bottom).

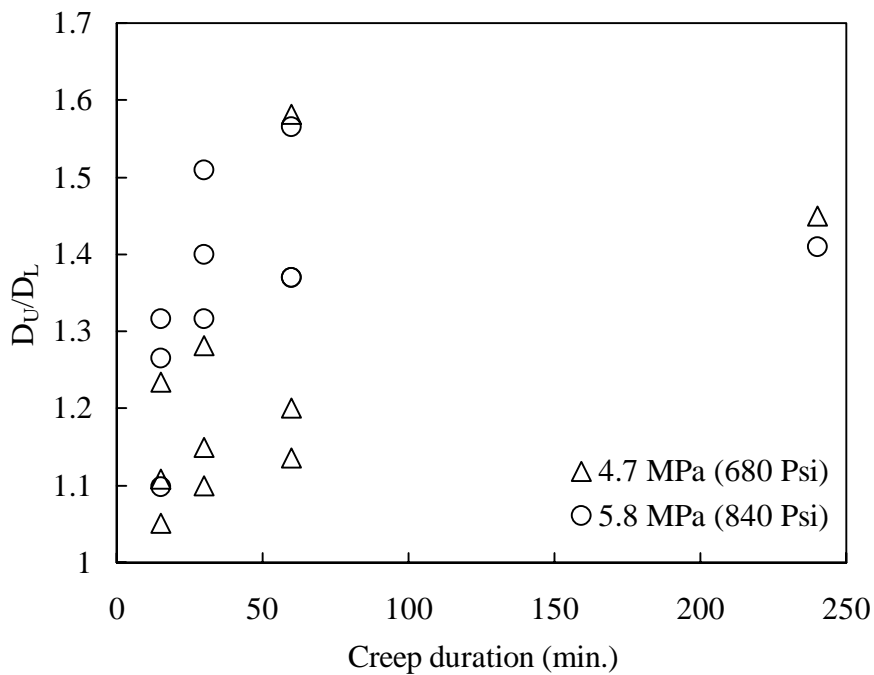
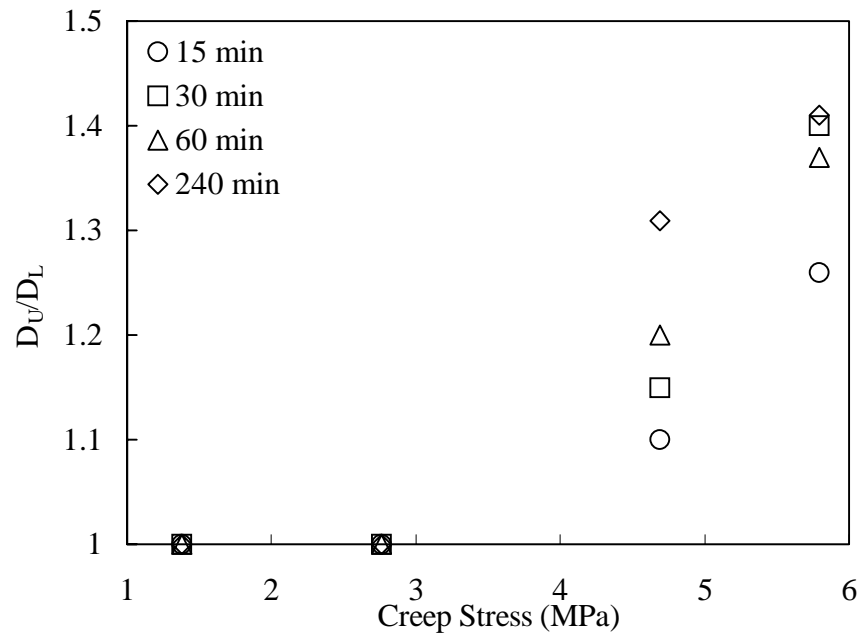


Fig. 6.3: Ratio of unloading and loading compliance as a function of creep stress (top) and duration (bottom) in the non-linear range

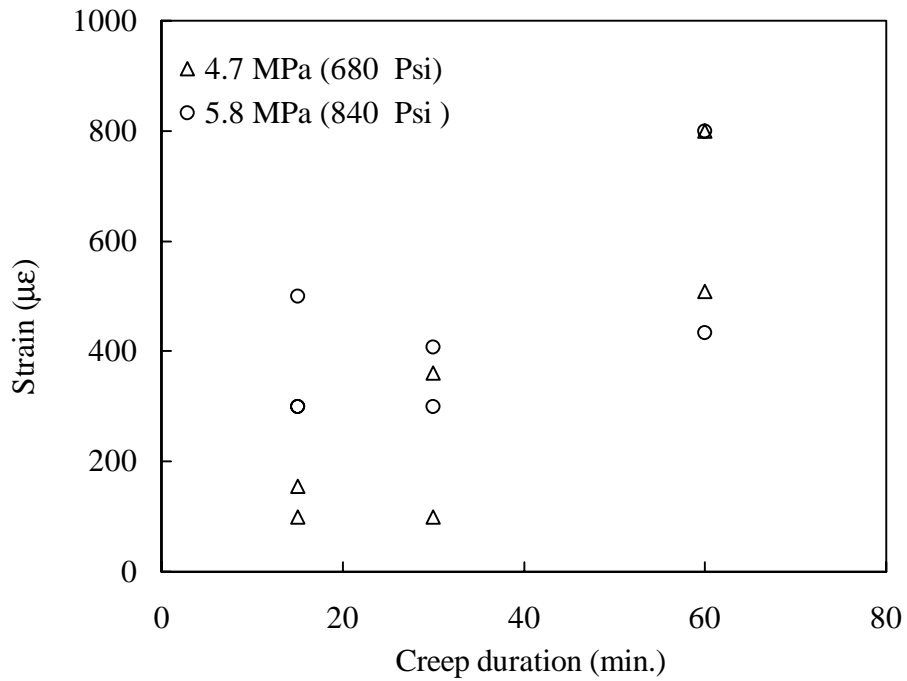
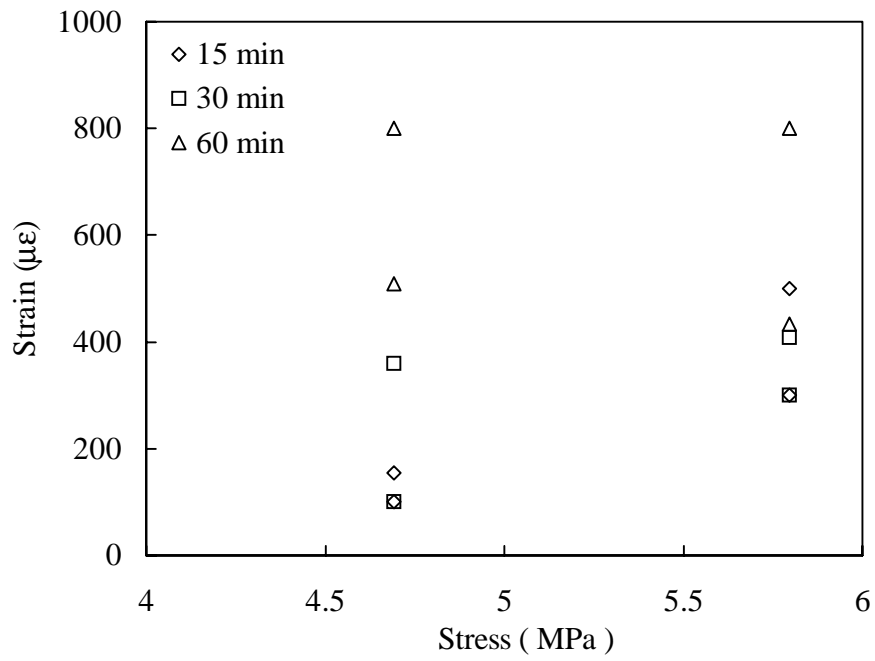


Fig. 6.4: Permanent strain as a function of creep stresses (top) and duration (bottom) in the non-linear range

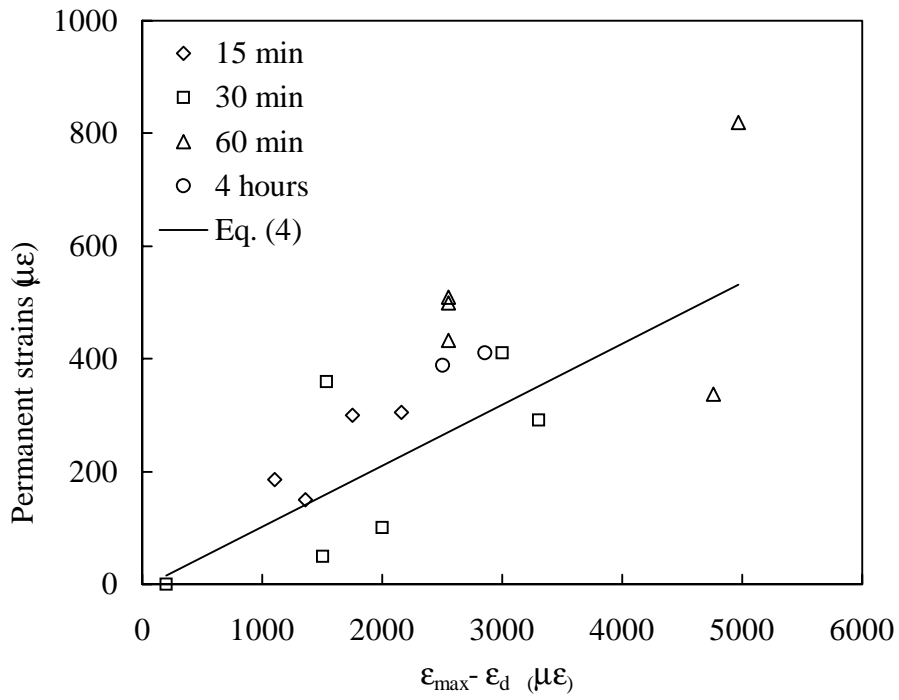


Fig. 6.5: Permanent strain as a function of maximum coupon strain.

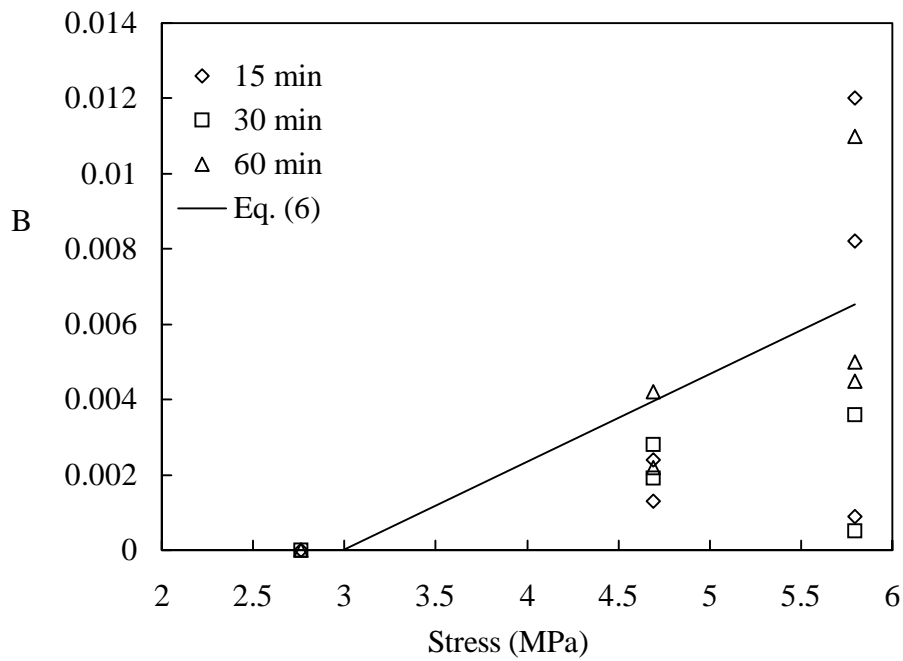
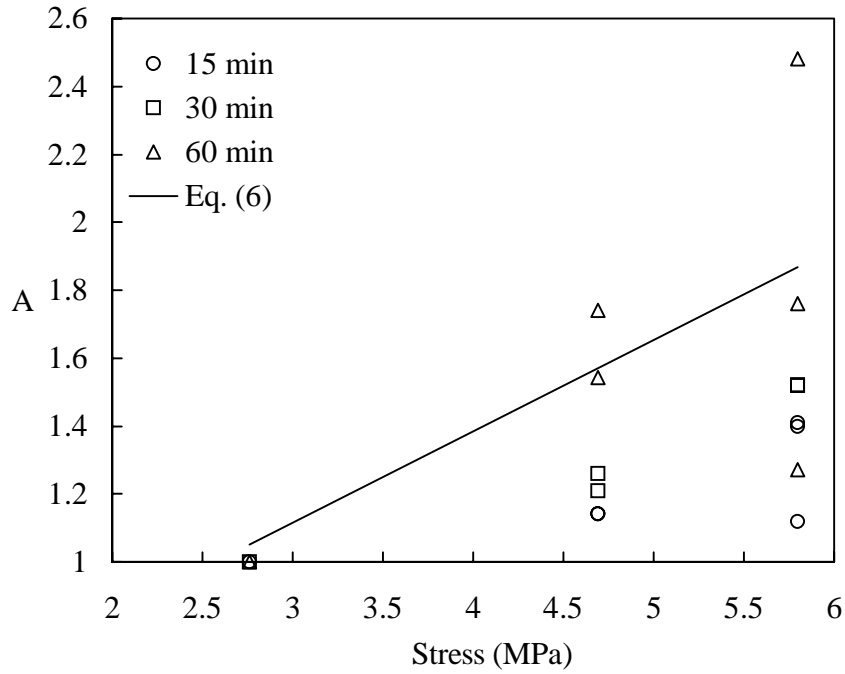


Fig. 6.6: Comparison between Eq.(6.6) and damage parameters A (top) and B (bottom) obtained from best fit for each coupon

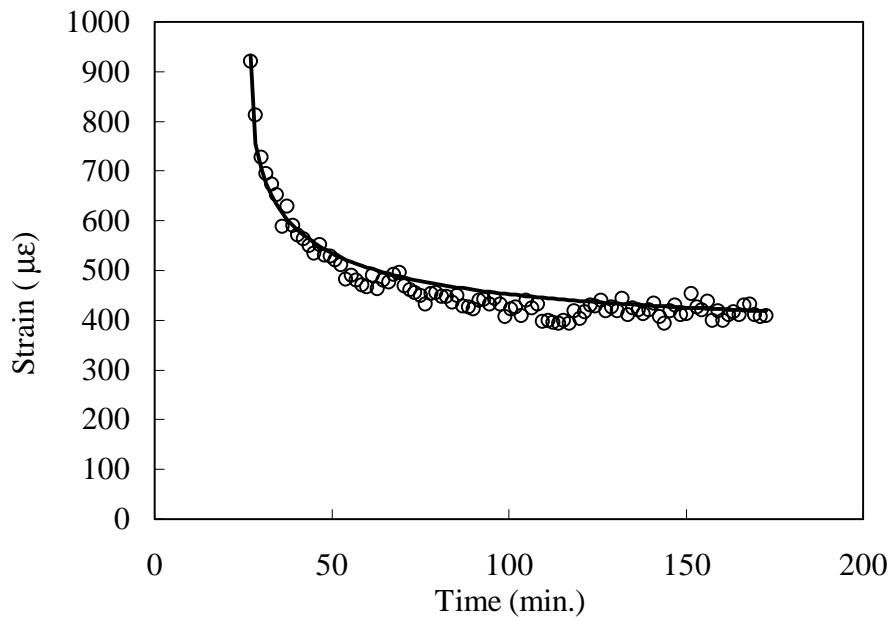
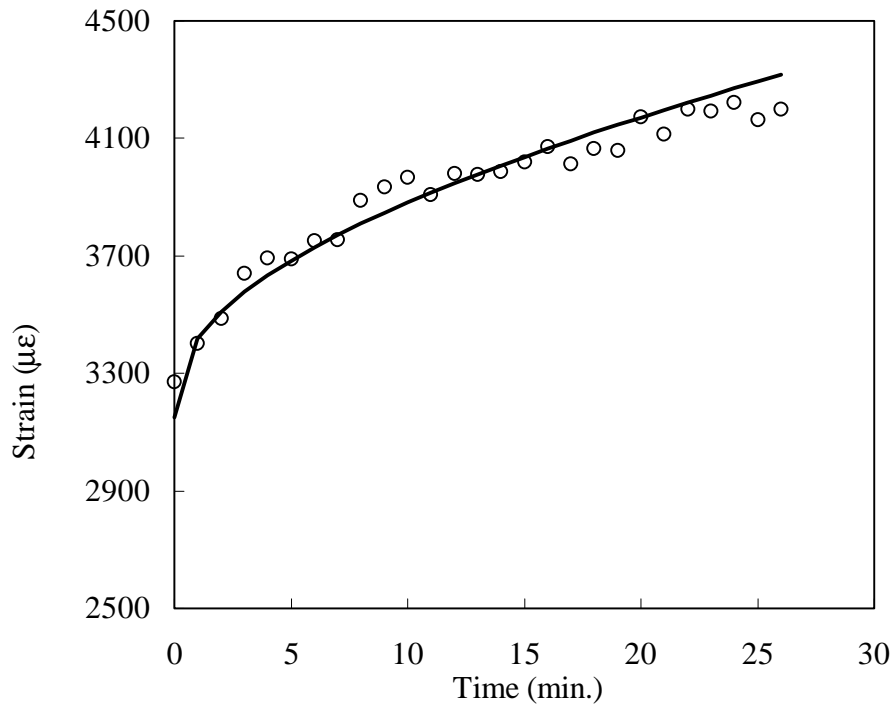


Fig. 6.7: Comparison between Eq.(6.10) and a representative coupon at a creep stress of 5.796 MPa (840 Psi) for creep (top) and recovery (bottom).

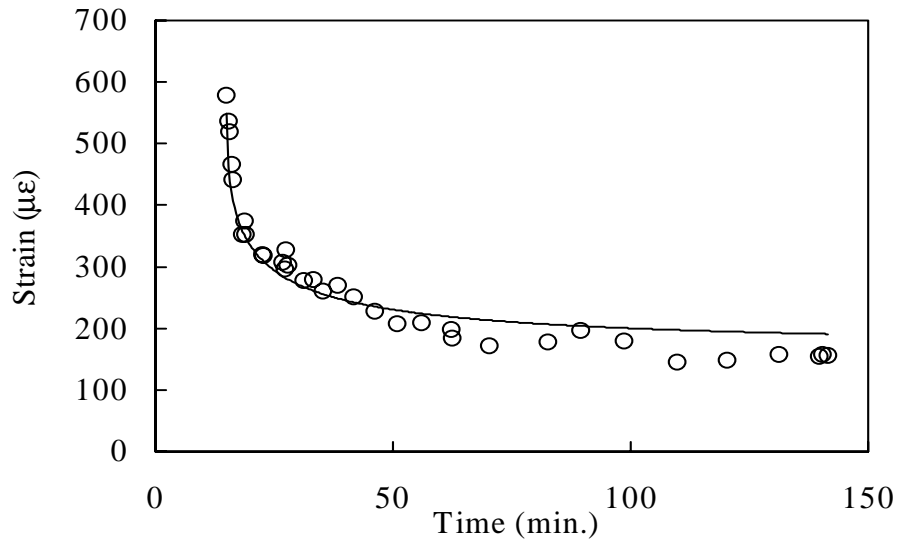
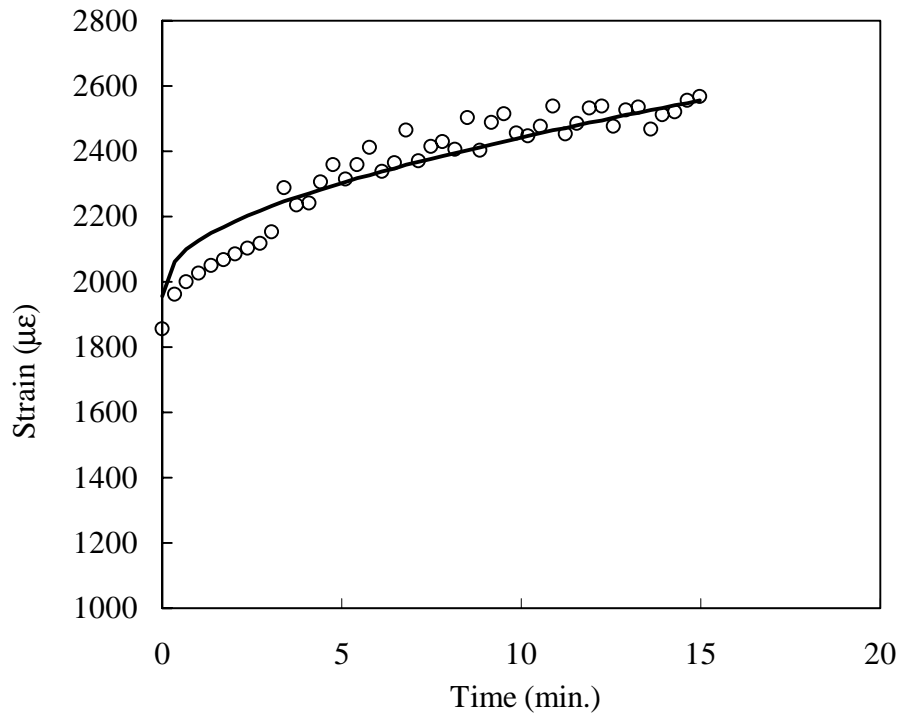


Fig. 6.8: Comparison of Eq.(6.10) and a representative coupon at a creep stress of 4.692 MPa (680 Psi) for creep (top) and recovery (bottom)

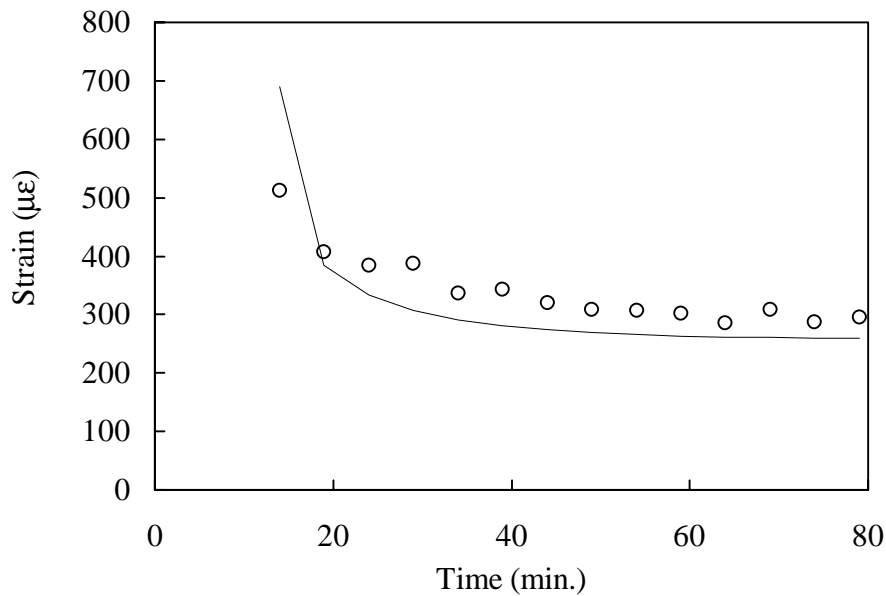
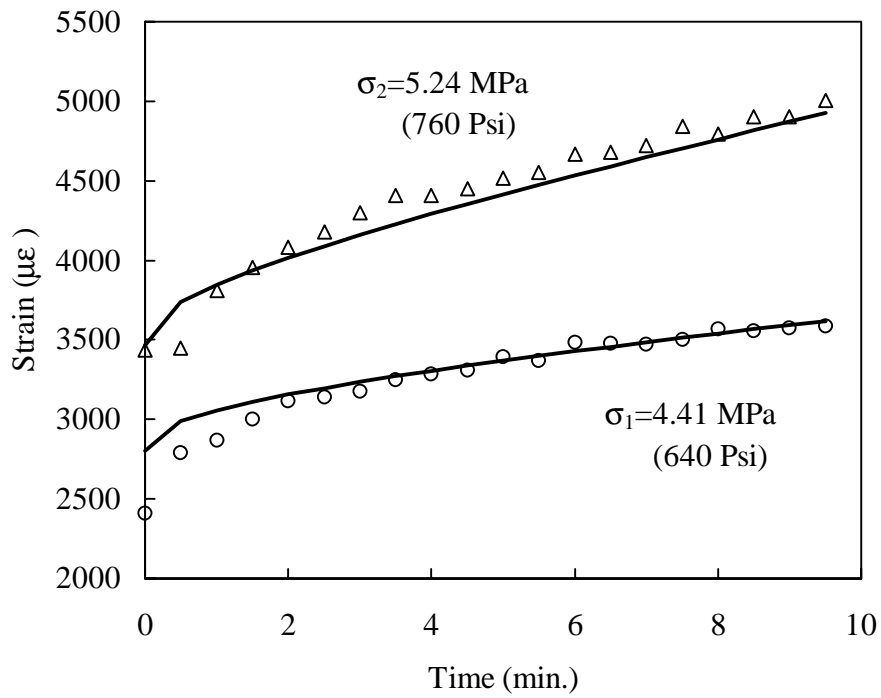


Fig. 6.9: Comparison between Eq. (6.15) and a representative coupon for the model verification test with $\sigma_2 > \sigma_1$, creep (top) and recovery for second step (bottom).

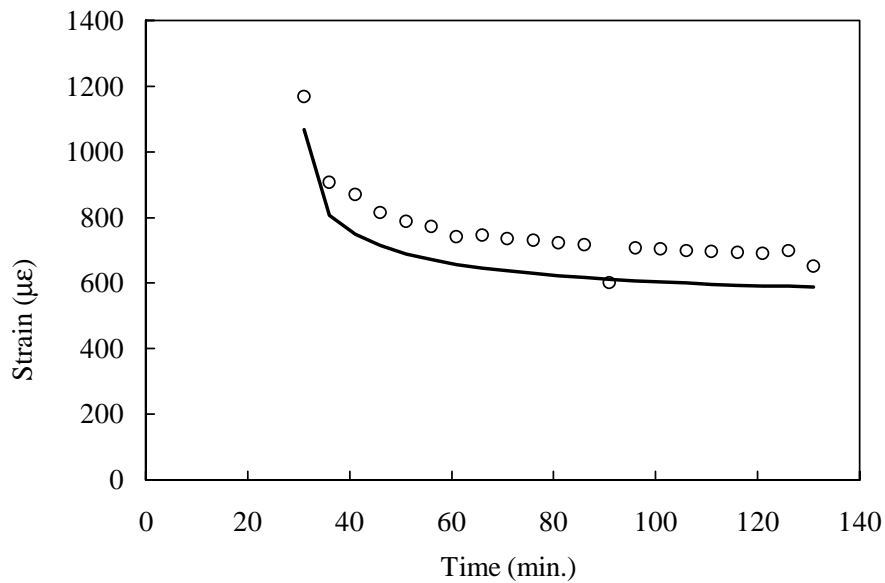
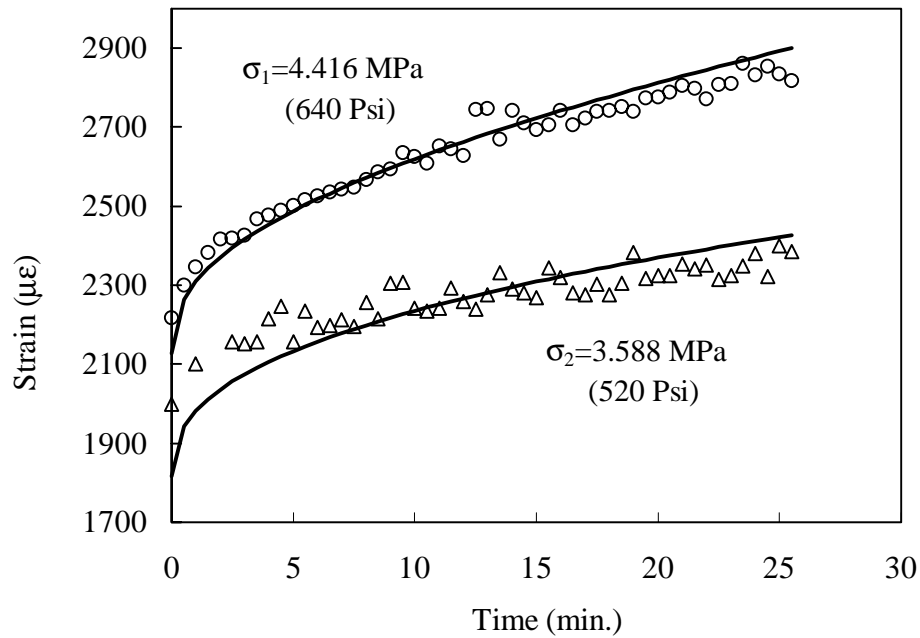


Fig 6.10: Comparison of Eq. (6.16) with a representative coupon for model verification test with $\sigma_2 < \sigma_1$, creep (top) and recovery for second step (bottom)

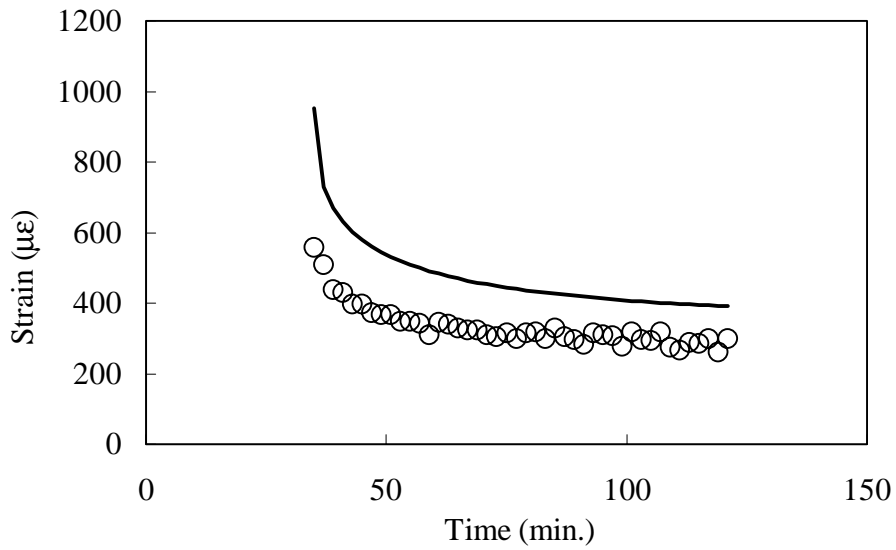
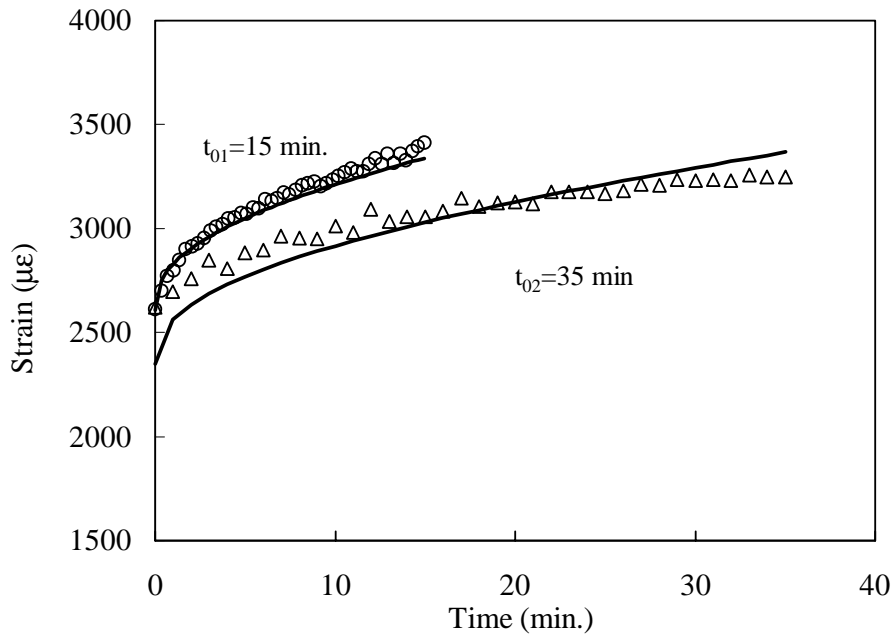


Fig. 6.11: Comparison between Eq. (6.16) and a representative coupon for a model verification test with $t_{02} > t_{01}$ and $\sigma_2 = \sigma_1$, creep (top) and recovery for second step (bottom).

CHAPTER EIGHT

SUMMARY AND FUTURE DIRECTION

Summary

Test methods and set-up for conducting durability studies on wood-thermoplastic composites were outlined. Results from such studies on three of the candidate materials were presented.

Moisture sorption process in these materials seemed to follow a linear Fickian response reasonably well. Moisture induced degradation in strength and stiffness was observed from static tests. Preliminary results from microscopic studies to qualitatively analyze this degradation were presented. Moisture sorption seemed to lower life in immersed fatigue and accelerates stiffness degradation. Reasonably good agreement was obtained between the proposed correlation for fatigue life and test data.

The power law based viscoelastic model represents the response of the material adequately well. The observed effects of damage and permanent deformation were incorporated into the model.

Recommendations

Techniques like X-Ray, C-Scan and Spate imaging may be used to qualitatively describe the origin and nature of damage accompanying fatigue and creep loading. Previous workers (Refs. 6.1, 6.2 and 6.3) have shown the success of these techniques in observing such effects. These studies may lead to better methods of accommodating the influence of damage into the durability models.

The manner in which the effect of damage has been incorporated into the viscoelastic model may limit its scope of applicability to the durations considered in this study. The form of the damage function would suggest that for all stresses exceeding the linear limit (σ_d), strains exhibit a switchover to tertiary creep. Data from relatively long duration creep tests must be compared with the model to check if this result is borne out. It is thought that the time dependence in the damage function should be more appropriately expressed by a power q , where $q < 1$. This modified form of the model should be validated with verification tests over a wide range of creep durations.

A model for damage accompanying fatigue loading must be developed. A framework for such a model has already been established as a part of this study, though not reported here. The damage progression during fatigue loading can be explained using the “mesoscale composite damage theory” of Ledveze, which is based on irreversible thermodynamics. Here, the goal is to predict the response of the material in the presence of damage that originates in the first few fatigue cycles and progresses with repeated fatigue cycling up to macroscopic crack initiation or failure. As damage occurs, the material loses stiffness and exhibits nonlinear, inelastic response.

Degradation of stiffness, is expressed in terms of a damage parameter that is a function of the associated thermodynamic force which serves as a damage evolution parameter. The modulus degradation (damage) parameter is the internal variable, and the thermodynamic force is the corresponding associated variable (in thermodynamic sense). The damage parameter must be empirically determined from test data.

With data on modulus degradation during fatigue loading available from the in-situ strain measurements, the damage parameter can be readily obtained as a function of

time (cycles) from a best-fit curve to the data of stiffness as a function of time (no. of cycles) during fatigue loading. The thermodynamic force governs damage development, a previous maximum value of some function of the thermodynamic forces must be exceeded for additional damage to occur. Failure can be described by a critical value of this thermodynamic force, thereby using stiffness degradation as a failure criterion.

The effects of moisture and temperature on viscoelastic response of the material must be investigated. Viscoplasticity and damage may be enhanced by moisture, these influences must be incorporated into the model. Moisture and temperature effects can be modeled using the time-moisture and time-temperature superposition principles.